J. Fluid Mech. (2023), *vol*. 963, A24, doi:10.1017/jfm.2023.336

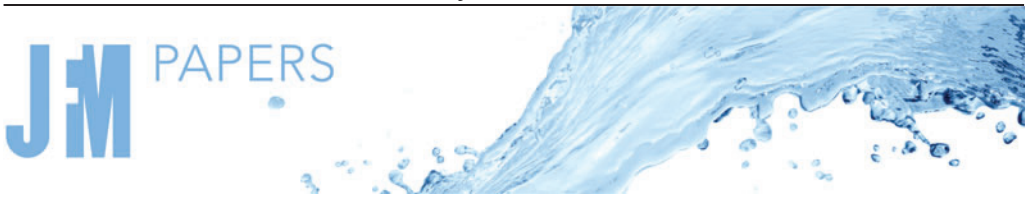

Resistive-force theory of slender bodies in viscosity gradients

Catherine Kamal[1],† **and Eric Lauga**[1],†

[1]Department of Applied Mathematics and Theoretical Physics, University of Cambridge, Cambridge CB3 0WA, UK

(Received 13 October 2022; revised 27 February 2023; accepted 10 April 2023)

In many natural settings, spatial variations in a fluid's viscosity arise due to changes in its local physico-chemical environment. We consider the low-Reynolds-number dynamics of slender bodies in fluids with a linearly varying viscosity. Assuming the spatial change in viscosity to be small compared to the spatial deviation of the body but large relative to the body's aspect ratio, we derive the modifications to resistive-force theory in a fluid due to a constant viscosity gradient. At leading order in the body slenderness, the results are identical to the classical theory in a constant-viscosity fluid but with the viscosity taking everywhere its local, non-constant value. At next order in slenderness, non-local terms arise due to the non-zero viscosity gradient. We use our results to predict the motion of straight and toroidal filaments settling under the action of gravity. We show that viscosity gradients induce rigid-body rotation of the filaments at a rate proportional to the components of the gradients along the filaments. This result contrasts with constant-viscosity fluids where the filaments do not rotate. We demonstrate further that if the viscosity gradient acts in the direction opposite to the gravitational field, then the filaments rotate towards a stable orientation, whose value depends on the ratio between the viscosity gradients parallel and perpendicular to the gravitational field; otherwise, the filaments align in the direction of the gravitational field. Our work shows that viscosity gradients can exert new forces on slender bodies, which could, for example, be used to control their orientation and drift.

Key words: slender-body theory

1. Introduction

From living organisms to passive particles, predicting the low-Reynolds-number resistance (or mobility) of bodies in viscous flow is fundamental in the field of colloidal science. Under the classical incompressible Stokes flow assumptions, exact solutions exist for a

† Email addresses for correspondence: ck620@cam.ac.uk, e.lauga@damtp.cam.ac.uk

few shapes, including the textbook example of a spherical body in an unbounded fluid (Stokes' solution), but challenges arise when it comes to the dynamics of elongated particles. Analytical expressions for the resistance coefficients of spheroids and ellipsoidal particles have been derived (Kim & Karrila 2013), and as such can be used to predict the resistance of elongated particles. Burgers (1938) was the first to attempt to predict the resistance of slender filaments in Stokes flow. He showed that the disturbance field of a slender body translating with uniform velocity is given to leading order by a constant line distribution of point forces over the body's length. His approach was developed in the 1960s and 1970s into what is now termed resistive-force theory (RFT), the leading-order slender-body theory used to approximate the dynamics of very slender particles (Tuck 1964; Batchelor 1970; Cox 1970, 1971; Tillett 1970). That theory leads to a locally linear and instantaneous, albeit tensorial, relationship between the velocity of a filament and the hydrodynamic forces exerted by the moving fluid. The predictions from RFT have since been used widely to approximate the mobility of both passive slender fibres (Du Roure *et al.* 2019) and living slender organisms (Brennen & Winet 1977; Lauga 2020).

The standard RFT formalism was derived assuming a Newtonian fluid with constant viscosity, but in many natural environments, patchiness and heterogeneity can often violate one or more of the classical assumptions assumed in Stokes flow. For example, spatial variations in the viscosity of a fluid can occur due to changes in temperature gradients or salt concentrations, such as in lakes and oceans (Arrigo *et al.* 1999), and changes in pH due to chemical reactions (Ottemann & Lowenthal 2002; Mirbagheri & Fu 2016) or through the mixing of different fluids such as mucus or extracellular polymeric substances. In addition, introducing external bodies into a fluid can also create local viscosity gradients when the particles have a temperature or chemical composition different to that of the background fluid (Han, Shields IV & Velev 2018). Recent microrheological studies have revealed the existence of viscosity gradients on the length scales of planktonic microorganisms, with up to 40-fold local increases in viscosity (Guadayol *et al.* 2021). In microbiology, viscosity gradients in mucus and other biological fluids play an important role in preventing pathogens, and these gradients affect the mobility of cells or other organisms inside the fluid (Swidsinski *et al.* 2007; Wheeler *et al.* 2019). Further, in what is termed viscotaxis, some pathogens, such as the bacteria *Spiroplasma* and *Leptospira interrogans* (Greenberg & Canale-Parola 1977; Petrino & Doetsch 1978; Daniels, Longland & Gilbart 1980; Takabe *et al.* 2017), and the microalga *Chlamydomonas reinhardtii* (Coppola & Kantsler 2021; Stehnach *et al.* 2021), have the ability to adapt their motion in viscosity gradients to migrate towards favourable regions of viscosity.

Viscotaxis has motivated recent theoretical and numerical studies of active and passive swimmers in viscosity gradients or media with spatially varying viscosity (Takabe *et al.* 2017; Liebchen *et al.* 2018; Datt & Elfring 2019; Laumann & Zimmermann 2019; Dandekar & Ardekani 2020; Eastham & Shoele 2020; López *et al.* 2021; Shaik & Elfring 2021; Stehnach *et al.* 2021). One important finding of these studies is the impact of viscosity changes on mobility. A linear force acting on two passive particles connected by a filament results in the particle migrating to regions of greater viscosity, while a nonlinear or chiral force results in the particles migrating to lower regions of viscosity (Liebchen *et al.* 2018). Spherical squirmers (Datt & Elfring 2019; Shaik & Elfring 2021) and soft passive particles in shear flow (Laumann & Zimmermann 2019) are also found to migrate towards lower regions of viscosity. A synthetic helical swimmer crossing a sharp viscosity gradient created by two miscible fluids has also been studied, both experimentally and theoretically (López *et al.* 2021), and it was found to be generally easier for a swimmer pulled from the front to swim towards higher regions of viscosity, and harder

for a swimmer pushed from the back. A theoretical study on the propulsion of Taylor's waving sheet found its locomotion to depend critically on the dimensionless Péclet number quantifying the convection-to-diffusion for the transport of the viscosity (Dandekar & Ardekani 2020); at high Péclet number, the sheet propelled to higher-viscosity regions with propulsion speed proportional to the magnitude of the viscosity gradient, while at smaller Péclet numbers, the direction of the sheet's propulsion is reversed.

In this paper, we focus on the dynamics of slender bodies in viscosity gradients. As a first step towards modelling direct hydrodynamic interactions in arbitrary viscosity fields, we derive here how to modify rigorously the classical constant-viscosity RFT to account for a viscosity field with a constant gradient (§ 2). In our calculation, the spatial change in viscosity is assumed to be small with respect to the spatial deviation of the filament, but large relative to the filament's width-to-length aspect ratio. We then show how to apply our modified RFT to examine the effect of a viscosity gradient on the resistance of motion of rigid filaments settling under the action of gravity (straight filament in § 3 and toroidal filament in § 4). In particular, in a uniform viscosity field, symmetric rigid bodies settle without rotating (Taylor 1967), but the presence of viscosity difference leads to asymmetric stresses exerted on the particle, which can induce reorientation. The results in this paper provide a basis to approximate the dynamics of passive and active slender particles in arbitrary viscosity gradient fields, provided that they are small compared to the relevant length scale for viscosity changes.

2. Resistive-force theory in a uniform viscosity gradient

2.1. *Set-up*

We consider a slender body placed in a fluid with a prescribed constant viscosity gradient

$$\eta(\boldsymbol{x}) = \eta_0 \left(1 + \tilde{\boldsymbol{\kappa}} \cdot \frac{\boldsymbol{x} - \boldsymbol{x}_0}{2a}\right). \tag{2.1}$$

Here, $\boldsymbol{x}_0$ represents the location at which the viscosity η equals the reference viscosity η_0, and $\tilde{\boldsymbol{\kappa}}$ is the constant viscosity gradient, made dimensionless using η_0 and the body's half-length a. The fluid is subject to an incompressible external flow field denoted by $\boldsymbol{u}^\infty$. In the limit of vanishing Reynolds number, the total velocity field $\boldsymbol{u}$ satisfies the incompressible Stokes equations

$$\nabla \cdot \left\{\eta(\boldsymbol{x})\left[\nabla \boldsymbol{u} + (\nabla \boldsymbol{u})^{\mathrm{T}}\right]\right\} = \nabla p, \quad \nabla \cdot \boldsymbol{u} = 0. \tag{2.2}$$

The slender body has half-length a and a circular cross-section with maximum radius b, as illustrated in figure 1. The width-to-length aspect ratio of the body, $\varepsilon = b/a$, is assumed to be small. We parametrise the body using a dimensionless arc length s running through its longitudinal centre (made dimensionless with respect to a). Under this parametrisation, the body's longitudinal centreline can thus be written as $a\,\tilde{\boldsymbol{R}}(s)$, where $-1 \leq s \leq 1$, and its radius is described by $b\,\tilde{\lambda}(s)$. We assume that the dimensionless radius $\tilde{\lambda}(s)$ is continuous and that the radii at the endpoints of the body are zero (i.e. $\tilde{\lambda}(-1) = \tilde{\lambda}(1) = 0$). Without loss of generality, we may set $\eta_0 = \eta(a\,\tilde{\boldsymbol{R}}(s = 0))$, i.e. we take the reference viscosity to be that at the instantaneous middle point of the filament. Unless otherwise stated, we carry out in what follows our derivation in a dimensionless form, non-dimensionalising all length scales by a, viscosity by η_0 (so that $\tilde{\eta} = \eta/\eta_0$), and velocity by a characteristic velocity U, with tilde signs used to represent the dimensionless variables.

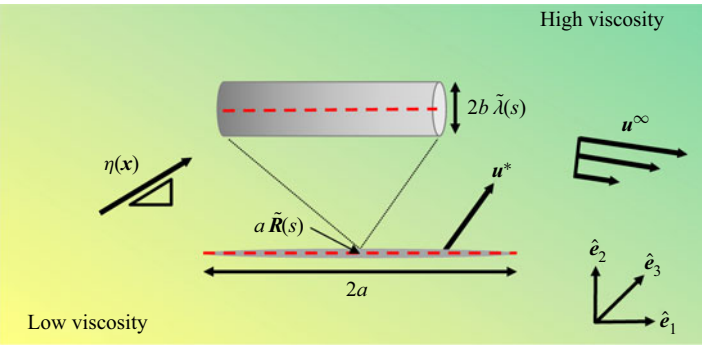

Figure 1. Sketch of a slender filament of length $2a$ and maximum radius b in an external velocity field $\boldsymbol{u}^{\infty}$ in a fluid with a linearly varying viscosity $\eta(\boldsymbol{x}) = \eta_0(1 + \tilde{\boldsymbol{\kappa}} \cdot (\boldsymbol{x} - \boldsymbol{x}_0)/(2a))$, where η_0 is the value of the viscosity at the instantaneous centre of the filament, and the constant viscosity gradient is denoted $\tilde{\boldsymbol{\kappa}}$. The red dashed line represents the body's centreline, located at $a\,\tilde{\boldsymbol{R}}(s)$, while the radius of the filament is denoted by $b\,\tilde{\lambda}(s)$. The gradient background represents the variation in viscosity schematically.

A classical approach used to compute the hydrodynamics of slender bodies in Stokes flows (Batchelor 1970) is to approximate the velocity field $\boldsymbol{u}$ by a line distribution of point forces of density $\boldsymbol{f}$ over the centreline $a\,\tilde{\boldsymbol{R}}(s)$. The effects of the edges on the leading force distribution are assumed to be subdominant.

We introduce the Green's function $\boldsymbol{G}^{V} \cdot \boldsymbol{f}\,\mathrm{d}\hat{s}/(8\pi)$ to represent the velocity field produced by a force density $\boldsymbol{f}$ spread over an infinitesimal length $\mathrm{d}\hat{s}$ in a viscous flow field with the prescribed viscosity field $\eta(\tilde{\boldsymbol{x}})$, where $\hat{s}$ is the dimensionless arc length integration variable. Since the viscosity field $\eta(\tilde{\boldsymbol{x}})$ is embedded into $\boldsymbol{G}^{V}$, the Green's function has dimensions of the inverse of viscosity. Non-dimensionalising as $G^{V}_{ij} \equiv \tilde{G}^{V}_{ij}/\eta_0$, the flow created by a continuous force density $\boldsymbol{f}$ is written as

$$u_i(\boldsymbol{x}) = \frac{1}{8\pi\eta_0}\int_{-1}^{1} \tilde{G}^{V}_{ij}(\tilde{\boldsymbol{x}} - \tilde{\boldsymbol{R}}(\hat{s}))\, f_j(\hat{s})\,\mathrm{d}\hat{s}, \tag{2.3}$$

where, up to leading order in the viscosity gradient $\tilde{\boldsymbol{\kappa}}$, the Green's function is given by (Laumann & Zimmermann 2019)

$$\tilde{G}^{V}_{ij}(\boldsymbol{x}') = \frac{1}{\tilde{\eta}(\hat{s})}\left[\left(\frac{\delta_{ij}}{X} + \frac{x_i' x_j'}{X^3}\right)\left(1 - \frac{\tilde{\kappa}_k x_k'}{4a\,\tilde{\eta}(\hat{s})}\right) + \frac{1}{4\tilde{\eta}(\hat{s})}\,\frac{x_i'\tilde{\kappa}_j - \tilde{\kappa}_i x_j'}{aX}\right], \quad X = |\boldsymbol{x}'|. \tag{2.4}$$

The objective is then to identify a suitable force density $\boldsymbol{f}$ so that (2.3) satisfies (2.2) along with the no-slip conditions $\boldsymbol{u}(s) = \boldsymbol{u}^{*}(s)$ along the surface of the body (where $\boldsymbol{u}^{*}(s)$ corresponds to the velocity averaged on the cross-section of the body).

The flow field in (2.3) is known to lead to a mathematical singularity if we model the filament as a line of vanishing thickness (Stokes paradox). To overcome this issue, the now-classical approach that leads to the results of RFT was proposed in the 1970s (Batchelor 1970; Cox 1970). The idea is to exploit the slenderness of the filament to match (2.3) at a point s on the centreline to an inner flow field that corresponds to the flow around a cylinder of infinite extent and radius $b\,\tilde{\lambda}(s)$ that satisfies the uniform no-slip condition $\boldsymbol{u}(s) = \boldsymbol{u}^{*}(s)$ on its surface. The case of a uniform viscosity field ($\eta = \eta_0$) has been solved in classical work (Batchelor 1970; Cox 1970), and in this paper, we expand on these studies.

Specifically, we follow closely the derivation of Cox (1970) to obtain a solution for $\boldsymbol{f}$ that depends on the curved shape of the centreline in a constant viscosity gradient. In our

derivation, we assume that the dimensionless viscosity gradient $\tilde{\boldsymbol{\kappa}}$ is small with respect to the spatial change in the length of the body. Since, as we see below, ε needs to be exponentially small for RFT to be valid (meaning that $|\ln\varepsilon|$ is an asymptotically large number), it also follows that $|\tilde{\boldsymbol{\kappa}}| \gg \varepsilon$. Moreover, since any spatial deviation of the relative viscosity $\eta(a\tilde{\boldsymbol{R}})/(\eta_0)$ along the radial direction away from the body's centreline (using the unit radial vector $\hat{\boldsymbol{e}}_\rho$ in local polar coordinates along the instantaneous centreline) is of the order of $(\tilde{\boldsymbol{\kappa}}\cdot\hat{\boldsymbol{e}}_\rho)\varepsilon$, the effects of a spatial change in the viscosity in the radial direction $\tilde{\boldsymbol{\kappa}}\cdot\hat{\boldsymbol{e}}_\rho$ can be ignored to leading order in the body slenderness. The only relevant spatial component of the dimensionless viscosity gradient $\tilde{\boldsymbol{\kappa}}$ therefore acts in the tangential direction along the centreline itself, i.e. the component $\tilde{\kappa}_1 = \tilde{\boldsymbol{\kappa}}\cdot\hat{\boldsymbol{e}}_1$, where $\hat{\boldsymbol{e}}_1$ denotes the local unit vector directed in the tangent to the centreline.

We proceed in evaluating the force density $\boldsymbol{f}$ by computing the leading correction due to $\tilde{\kappa}_1$ to the inner flow field (§ 2.2) and the outer flow field for a uniform viscosity field (§ 2.3).

2.2. *Inner solution*

Following the calculation in Cox (1970), the inner solution $\tilde{\boldsymbol{u}}^{in}$ is found by focusing on an arbitrary point s on the surface of the filament s on the surface of the filament. Given that the filament is slender, on the relevant length scale b, we have $b \ll a$ and thus the filament appears locally to be a cylinder of circular cross-section and infinite extent, as sketched in figure 1. The radius of the cylinder is therefore approximately uniform. Using dimensionless polar coordinates $(\bar{\rho}, \theta, \bar{x}_1)$, the surface of the cylinder $\bar{\boldsymbol{x}}$ can be parametrised using inner variables as

$$\bar{\boldsymbol{x}} = \bar{x}_1\,\hat{\boldsymbol{e}}_1 + \bar{\rho}\cos\theta\,\hat{\boldsymbol{e}}_2 + \bar{\rho}\sin\theta\,\hat{\boldsymbol{e}}_3, \quad \bar{\rho} = \tilde{\lambda}(s) + O(\varepsilon), \quad \bar{x}_1 = s + O(\varepsilon), \tag{2.5}$$

about an orthogonal coordinate system with $\hat{\boldsymbol{e}}_1$, $\hat{\boldsymbol{e}}_2$ and $\hat{\boldsymbol{e}}_3$ directed in the direction of the tangent, normal and binormal of the centreline at s, respectively. Here, $\bar{(\cdot)}$ is used to denote the inner (dimensionless) variables, and we use $\tilde{(\cdot)}$ for the outer (dimensionless) variables. The inner flow $\tilde{\boldsymbol{u}}^{in}$ must satisfy (2.2) with the no-slip boundary conditions on the body surface, i.e.

$$\tilde{\boldsymbol{u}}^{in}(\bar{\boldsymbol{x}}) = \tilde{\boldsymbol{u}}^{*}(s). \tag{2.6}$$

We wish to solve the inner solution up to the leading order correction in $\tilde{\kappa}_1$ for a varying viscosity gradient. We thus solve for the velocity and pressure fields as expansions $\tilde{\boldsymbol{u}}^{in} = \tilde{\boldsymbol{u}}_0^{in}(\tilde{\kappa}_1) + O(\varepsilon)$ and $\tilde{p}^{in} = \tilde{p}_0^{in}(\tilde{\kappa}_1) + O(\varepsilon)$.

At the inner scale, the spatial change in the viscosity at a point $\bar{\boldsymbol{x}}$ on the surface is of the order of $\tilde{\kappa}_1(\bar{x}_1 - s) \sim O(\tilde{\kappa}_1\varepsilon)$. Therefore, the leading-order correction to $\tilde{\boldsymbol{u}}^{in}$ due to the viscosity change $\tilde{\boldsymbol{\kappa}}$ is asymptotically smaller than the zeroth-order solution for $\tilde{\boldsymbol{u}}_0^{in}$ in a uniform viscosity field with dimensionless viscosity taken to be $\tilde{\eta}_s \equiv \tilde{\eta}(\tilde{\boldsymbol{R}}(s))$ at each point along the centreline. The leading-order solution for $\tilde{\boldsymbol{u}}^{in}$ in both ε and $\tilde{\boldsymbol{\kappa}}$ is thus exactly the same as that derived by Cox (1970) but with $\tilde{\eta}_0$ (which is equal to unity) formally interchanged with $\tilde{\eta}_s$.

Re-writing the expression for $\tilde{\boldsymbol{u}}^{in}$ using the outer variables $\tilde{\rho} = \varepsilon\bar{\rho}$ and $\tilde{x} = \varepsilon\bar{x}$ gives the inner boundary condition on the outer flow field $\tilde{\boldsymbol{u}}$ in the inner limit $\tilde{\rho} \to 0$, up to leading

order in ε and $\tilde{\kappa}_1$:

$$\left.\begin{aligned}
\tilde{u}_z &= E(\varepsilon)\ln(\tilde{\rho}/\tilde{\lambda}) + \tilde{u}_1^*,\\
\tilde{u}_{\tilde{\rho}} &= \tilde{u}_2^*\cos\theta + \tilde{u}_3^*\sin\theta + (1-\tilde{\lambda}^2\tilde{\rho}^{-2} - 2\ln(\tilde{\rho}/\tilde{\lambda}))(C(\varepsilon)\cos\theta + D(\varepsilon)\sin\theta),\\
\tilde{u}_\theta &= -\tilde{u}_2^*\sin\theta + \tilde{u}_3^*\cos\theta + (-1+\tilde{\lambda}^2\tilde{\rho}^{-2} - 2\ln(\tilde{\rho}/\tilde{\lambda}))(D(\varepsilon)\cos\theta - C(\varepsilon)\sin\theta),\\
\tilde{p} &= \frac{4}{\tilde{\rho}}\,(C(\varepsilon)\cos\theta + D(\varepsilon)\sin\theta) + F(\varepsilon).
\end{aligned}\right\} \tag{2.7}$$

Here, C, D, E and F are dimensionless coefficients that depend on ε, still to be determined.

2.3. *Outer solution and matching*

The calculation of the outer solution, and the matching with the inner solution, is computed analogously to Cox (1970). The method requires first expanding the coefficients C, D, E and F from (2.7) to leading order in $1/\ln\varepsilon$, and then equating each order of the expansion to the outer flow and pressure field. The expansion of the outer flow field to $O((\ln\varepsilon)^{-1})$ is written formally as

$$\tilde{\boldsymbol{u}} = \tilde{\boldsymbol{u}}^{\infty} + \tilde{\boldsymbol{u}}^{(1)}/\ln\varepsilon. \tag{2.8}$$

The leading-order terms in (2.7) are first equated with the leading-order velocity $\tilde{\boldsymbol{u}}^{\infty} - \tilde{\boldsymbol{u}}^*$. At $O((\ln\varepsilon)^{-1})$, the outer flow field at the point at $\tilde{\boldsymbol{R}}(s)$ corresponds to the leading distribution of point forces as $\varepsilon \to 0$. Matching (2.7) to a line distribution of dimensionless point forces on $\tilde{\boldsymbol{R}}(s)$ with density $\tilde{\boldsymbol{f}}(s)$ as $\tilde{\rho} \to 0$ requires the outer force density to be (Cox 1970)

$$\tilde{\boldsymbol{f}}(s) = 4\pi\,\tilde{\eta}_s(\tilde{\boldsymbol{u}}^{\infty}(\tilde{\boldsymbol{R}}) - \tilde{\boldsymbol{u}}^*(s))\cdot\left(\boldsymbol{I} - \frac{1}{2}\frac{\mathrm{d}\tilde{\boldsymbol{R}}}{\mathrm{d}s}\frac{\mathrm{d}\tilde{\boldsymbol{R}}}{\mathrm{d}s}\right). \tag{2.9}$$

Here, we have assumed that $\hat{\boldsymbol{e}}_2$ lies in the same plane as $\hat{\boldsymbol{e}}_1$ and $\tilde{\boldsymbol{u}}^{\infty}(\tilde{\boldsymbol{R}}) - \tilde{\boldsymbol{u}}^*(s)$, so that the unit vectors $\hat{\boldsymbol{e}}_1, \hat{\boldsymbol{e}}_2, \hat{\boldsymbol{e}}_3$ can be expressed in terms of $\tilde{\boldsymbol{u}}^{\infty}(\tilde{\boldsymbol{R}}) - \tilde{\boldsymbol{u}}^*(s)$ and $\mathrm{d}\tilde{\boldsymbol{R}}(s)/\mathrm{d}s$ (Cox 1970).

The flow field $\tilde{\boldsymbol{u}}^{(1)}$ can then be obtained as that produced by the distribution of point forces with density $\tilde{\boldsymbol{f}}$ to leading order, analogously to (2.3). It is thus written as

$$\tilde{u}_i^{(1)} = \lim_{\tilde{\rho}\to 0}\frac{1}{2}\int_{-1}^{1}\tilde{G}_{ij}^{V}\left(\tilde{\boldsymbol{x}}'\right)\tilde{f}_j(\hat{s})\,\mathrm{d}\hat{s}, \quad \tilde{\boldsymbol{x}}' = \tilde{\boldsymbol{x}}(s) - \tilde{\boldsymbol{x}}(\hat{s}). \tag{2.10}$$

The only (but important) difference from the Cox (1970) derivation is with the definition of the tensor $\tilde{\boldsymbol{G}}^{V}$, where here $\tilde{\boldsymbol{G}}^{V}$ accounts for the prescribed viscosity gradient $\tilde{\boldsymbol{\kappa}}$, as given in (2.4).

Since we are interested in only the leading-order terms in ε, we can simplify the tensor $\tilde{G}_{ij}^{V}$ in (2.10) further by noting that in the spatial region of the integrand, we have $1/\tilde{\eta}(\hat{s}) \approx (1/\tilde{\eta}_s)(1 + \tilde{\boldsymbol{\kappa}}\cdot(\tilde{\boldsymbol{x}}'/2))$. Under this assumption, the tensor in (2.4) becomes, to

leading order in $\tilde{\boldsymbol{\kappa}}$ and ε,

$$\tilde{G}^V_{ij}(\boldsymbol{x}') = \frac{1}{\tilde{\eta}_s}\left[\left(\frac{\delta_{ij}}{X'} + \frac{x_i' x_j'}{X'^3}\right)\left(1 + \frac{\tilde{\kappa}_k x_k'}{4a}\right) + \frac{1}{4}\frac{x_i'\tilde{\kappa}_j - \tilde{\kappa}_i x_j'}{aX'}\right] + O(\tilde{\boldsymbol{\kappa}}^2, \varepsilon). \tag{2.11}$$

To evaluate the flow from (2.10), we let $\tilde{\boldsymbol{u}}^{(1)} = \boldsymbol{J}^* + \boldsymbol{J}$, where $\boldsymbol{J}^*$ denotes the integral over the singular part of the integrand in (2.10) taken over the region $[s-\epsilon, s+\epsilon]$ (where ϵ is an arbitrary number such that $\epsilon \ll 1$), and $\boldsymbol{J}$ is the integral on the remaining part of the line. Since $\epsilon \ll 1$, $\boldsymbol{J}^*$ can be evaluated analytically in the singular region of the integral as

$$J_i^* = \lim_{\tilde{\rho}\to 0}\frac{\tilde{\eta}_s}{2}(\tilde{u}_k^{\infty}(\hat{R}) - \tilde{u}_k^*(s))\left(\delta_{jk} - \frac{1}{2}\frac{\mathrm{d}\tilde{R}_j}{\mathrm{d}s}\frac{\mathrm{d}\tilde{R}_k}{\mathrm{d}s}\right)\int_{s-\epsilon}^{s+\epsilon}\tilde{G}^V_{ij}\left(\tilde{\boldsymbol{x}}'\right)\mathrm{d}\hat{s}. \tag{2.12}$$

We can further simplify $\tilde{\boldsymbol{G}}^V$ in this singular region. Since $\tilde{\boldsymbol{x}}(\hat{s}) \approx \hat{s}\hat{\boldsymbol{e}}_1$, we have $\tilde{\boldsymbol{x}}(s) = (s, \tilde{\rho}\cos\theta, \tilde{\rho}\sin\theta)$ and $\tilde{\boldsymbol{x}}(\hat{s}) = (\hat{s}, \tilde{\rho}\cos\theta, \tilde{\rho}\sin\theta)$. Recalling that the only contribution in $\tilde{\boldsymbol{\kappa}}$ with terms of order greater than ε comes from $\tilde{\boldsymbol{\kappa}}\cdot\hat{\boldsymbol{e}}_1 = \tilde{\kappa}_1$, we obtain

$$\tilde{G}^V_{ij}(\boldsymbol{x}') = \frac{1}{\tilde{\eta}_s}\left[\left(\frac{\delta_{ij}}{X'} + \frac{x_i' x_j'}{X'^3}\right)\left(1 + \frac{\tilde{\kappa}_1 x_1'}{4a}\right) + \frac{1}{4}\frac{x_i'\tilde{\kappa}_j\delta_{1j} - \tilde{\kappa}_i x_j'\delta_{1i}}{aX'}\right] + O(\tilde{\boldsymbol{\kappa}}^2, \varepsilon). \tag{2.13}$$

The integral in (2.12) can be evaluated analytically by introducing

$$M_{ij}^* = \lim_{\tilde{\rho}\to 0}\int_{s-\epsilon}^{s+\epsilon}\tilde{G}^V_{ij}\left(\tilde{\boldsymbol{x}}'\right)\mathrm{d}\hat{s}, \tag{2.14}$$

with

$$M_{xx}^* = \frac{1}{\tilde{\eta}_s}\left(4\ln\left(\frac{2\epsilon}{\tilde{\rho}}\right) - 2\right) + O(\varepsilon\tilde{\boldsymbol{\kappa}}, \varepsilon), \tag{2.15}$$

$$M_{yy}^* = \frac{1}{\tilde{\eta}_s}\left(2\ln\left(\frac{2\epsilon}{\tilde{\rho}}\right) + 2\cos^2\theta\right) + O(\varepsilon\tilde{\boldsymbol{\kappa}}, \varepsilon), \tag{2.16}$$

$$M_{zz}^* = \frac{1}{\tilde{\eta}_s}\left(2\ln\left(\frac{2\epsilon}{\tilde{\rho}}\right) + 2\sin^2\theta\right) + O(\varepsilon\tilde{\boldsymbol{\kappa}}, \varepsilon), \tag{2.17}$$

$$M_{yz}^* = M_{zy}^* = \frac{2}{\tilde{\eta}_s}\sin\theta\cos\theta + O(\varepsilon\tilde{\boldsymbol{\kappa}}, \varepsilon), \tag{2.18}$$

$$M_{xy}^* = M_{yx}^* = O(\varepsilon\tilde{\boldsymbol{\kappa}}, \varepsilon), \tag{2.19}$$

$$M_{xz}^* = M_{zx}^* = O(\varepsilon\tilde{\boldsymbol{\kappa}}, \varepsilon). \tag{2.20}$$

It is important to note that all integrated terms containing $\tilde{\kappa}_1$ either vanish over the region $[s-\epsilon, s+\epsilon]$, or are of the order $O(\varepsilon\tilde{\kappa}_1)$. Therefore, $\boldsymbol{J}^*$ is the same as for the classical case of a constant viscosity up to order $O(\varepsilon\tilde{\boldsymbol{\kappa}}, \varepsilon)$, but with the addition of the prefactor $1/\tilde{\eta}_s$ for the varying viscosity.

Since the leading-order contribution of $\tilde{\kappa}_1$ enters only in the non-singular part of the integral, $\boldsymbol{J}$, the dimensionless outer flow $\tilde{\boldsymbol{u}}^{(1)}$, pressure $\tilde{p}^{(1)}$ and force density $\bar{\boldsymbol{f}}(s)$ can be expressed in the same way as in Cox (1970) for a uniform viscosity field. Namely, equating

(2.7)–(2.8) for $\tilde{\rho} \to 0$, one obtains the coefficients in (2.7) to be

$$C(\varepsilon) = \frac{1}{\ln \varepsilon}\frac{1}{2}(\tilde{u}_2^{\infty} - \tilde{u}_2^{*}) + \frac{1}{(\ln \varepsilon)^2}\frac{1}{4}(\tilde{u}_2^{\infty} - \tilde{u}_2^{*})\left(1 + 2\ln\left(\frac{2\epsilon}{\tilde{\lambda}}\right) + J_2\right) + O((\ln \varepsilon)^{-3}, \tilde{\boldsymbol{\kappa}}\varepsilon(\ln \varepsilon)^{-1}), \tag{2.21}$$

$$D(\varepsilon) = \frac{1}{(\ln \varepsilon)^2}\frac{J_3}{2} + O((\ln \varepsilon)^{-3}, \tilde{\boldsymbol{\kappa}}\varepsilon(\ln \varepsilon)^{-1}), \tag{2.22}$$

$$E(\varepsilon) = -\frac{1}{\ln \varepsilon}(\tilde{u}_1^{\infty} - \tilde{u}_1^{*}) + \frac{1}{(\ln \varepsilon)^2}\frac{1}{2}(\tilde{u}_1^{\infty} - \tilde{u}_1^{*})\left(1 - 2\ln\left(\frac{2\epsilon}{\tilde{\lambda}}\right) - J_1\right) + O((\ln \varepsilon)^{-3}, \tilde{\boldsymbol{\kappa}}\varepsilon(\ln \varepsilon)^{-1}). \tag{2.23}$$

The integral $\boldsymbol{J}$ is defined as

$$J_i = \lim_{\epsilon \to 0}\frac{\tilde{\eta}_s}{2}\left[\int_{-1}^{s-\epsilon} + \int_{s+\epsilon}^{1}\right]\tilde{G}_{ij}^{V}(\tilde{\boldsymbol{x}}(s) - \tilde{\boldsymbol{x}}(\hat{s}))\left(\delta_{jk} - \frac{1}{2}\frac{\mathrm{d}\hat{R}_j}{\mathrm{d}\hat{s}}\frac{\mathrm{d}\hat{R}_k}{\mathrm{d}\hat{s}}\right)(\tilde{u}_k^{\infty}(\hat{R}) - \tilde{u}_k^{*}(\hat{s}))\,\mathrm{d}\hat{s}, \tag{2.24}$$

where $\hat{R}_i = \tilde{R}_i(\hat{s})$.

2.4. *Force distribution*

As shown by Cox (1970), the force distribution can be evaluated explicitly from (2.7) and (2.21)–(2.23) to give

$$\bar{\boldsymbol{f}}(s) = 2\pi\,\tilde{\eta}_s(\tilde{\boldsymbol{\kappa}})\left[\frac{\tilde{\boldsymbol{u}}^{\infty} - \tilde{\boldsymbol{u}}^{*}}{\ln \varepsilon} + \frac{\boldsymbol{J}(\tilde{\boldsymbol{\kappa}}) + (\tilde{\boldsymbol{u}}^{\infty} - \tilde{\boldsymbol{u}}^{*})\ln(2\epsilon/\tilde{\lambda})}{(\ln \varepsilon)^2}\right]\cdot\left[\frac{\mathrm{d}\tilde{\boldsymbol{R}}}{\mathrm{d}s}\frac{\mathrm{d}\tilde{\boldsymbol{R}}}{\mathrm{d}s} - 2\boldsymbol{I}\right] + \frac{\tilde{\boldsymbol{u}}^{\infty} - \tilde{\boldsymbol{u}}^{*}}{2(\ln \varepsilon)^2}\cdot\left[3\frac{\mathrm{d}\tilde{\boldsymbol{R}}}{\mathrm{d}s}\frac{\mathrm{d}\tilde{\boldsymbol{R}}}{\mathrm{d}s} - 2\boldsymbol{I}\right] + O((\ln \varepsilon)^{-3}, \tilde{\boldsymbol{\kappa}}\varepsilon(\ln \varepsilon)^{-1}). \tag{2.25}$$

Crucially, the only differences between our results and the derivation from Cox (1970) are that the correction due to the viscosity gradient $\tilde{\boldsymbol{\kappa}}$ enters through $\tilde{\eta}_s(\tilde{\boldsymbol{\kappa}})$ and $\boldsymbol{J}(\tilde{\boldsymbol{\kappa}})$.

Finally, with the knowledge of $\bar{\boldsymbol{f}}(s)$ in (2.25), the total hydrodynamic force $\boldsymbol{F}$, torque $\boldsymbol{T}$ and stresslet $\boldsymbol{S}$ are

$$F_i = a\eta_0 U\int_{-1}^{1}\bar{f}_i(s)\,\mathrm{d}s, \tag{2.26}$$

$$T_i = a^2\eta_0 U\int_{-1}^{1}[\tilde{\boldsymbol{R}}(s)\times\bar{\boldsymbol{f}}(s)]_i\,\mathrm{d}s, \tag{2.27}$$

$$S_{ij} = a^2\eta_0 U\int_{-1}^{1}\tilde{R}_i(s)\bar{f}_j(s) + \tilde{R}_j(s)\bar{f}_i(s)]\,\mathrm{d}s, \tag{2.28}$$

where in the expression for $\boldsymbol{S}$, we have assumed that the centreline of the slender body is not deforming with time.

3. Straight filament in a linear viscosity gradient

To illustrate the effects of spatial variation in the viscosity on a fundamental example, we now use our modified RFT to estimate the leading-order forces and torques acting on slender straight filaments held fixed in different external flow fields.

3.1. *Uniform flow field*

We begin here by focusing on a straight filament of length $2a$, which is held fixed in a uniform flow field $\boldsymbol{u}^{\infty} = U_1\hat{\boldsymbol{e}}_1 + U_2\hat{\boldsymbol{e}}_2$ with constant viscosity gradient $\tilde{\boldsymbol{\kappa}}$. Without loss of generality, we may assume that the filament is held fixed with $\tilde{\boldsymbol{R}}(s) = s\hat{\boldsymbol{e}}_1$, hence $\mathrm{d}\tilde{\boldsymbol{R}}/\mathrm{d}s = \hat{\boldsymbol{e}}_1$.

3.1.1. *Computation of forces and torques*

Under this parametrisation, (2.24) becomes

$$J_i = \frac{\tilde{\eta}_s}{2}\left[\int_{-1}^{s-\epsilon} + \int_{s+\epsilon}^{1}\right]\tilde{G}^V_{ij}\left(s-\hat{s},0,0\right)\left(\frac{\tilde{U}_1}{2}\,\delta_{j1} + \tilde{U}_2\,\delta_{j2}\right)\mathrm{d}\hat{s}. \tag{3.1}$$

Here, we have dimensionalised U_1 and U_2 by a typical speed U. This integral can be evaluated analytically using

$$M_{ij} = \left[\int_{-1}^{s-\epsilon} + \int_{s+\epsilon}^{1}\right]\tilde{G}^V_{ij}\left(s-\hat{s},0,0\right)\mathrm{d}\hat{s}, \tag{3.2}$$

and its components are

$$M_{xx} = \frac{2}{\tilde{\eta}_s}\left(\ln(1-s^2) - 2\ln\epsilon + \frac{\tilde{\kappa}_1}{2}\,s\right) + O(\varepsilon\tilde{\boldsymbol{\kappa}},\varepsilon), \tag{3.3}$$

$$M_{yy} = \frac{1}{\tilde{\eta}_s}\left(\ln(1-s^2) - 2\ln\epsilon + \frac{\tilde{\kappa}_1}{2}\,s\right) + O(\varepsilon\tilde{\boldsymbol{\kappa}},\varepsilon), \tag{3.4}$$

$$M_{zz} = \frac{1}{\tilde{\eta}_s}\left(\ln(1-s^2) - 2\ln\epsilon + \frac{\tilde{\kappa}_1}{2}\,s\right) + O(\varepsilon\tilde{\boldsymbol{\kappa}},\varepsilon), \tag{3.5}$$

$$M_{yz} = M_{zy} = O(\varepsilon\tilde{\boldsymbol{\kappa}},\varepsilon), \tag{3.6}$$

$$M_{xy} = M_{yx} = O(\varepsilon\tilde{\boldsymbol{\kappa}},\varepsilon), \tag{3.7}$$

$$M_{xz} = M_{zx} = O(\varepsilon\tilde{\boldsymbol{\kappa}},\varepsilon). \tag{3.8}$$

The integral in (3.1) then becomes

$$J_i = \frac{\tilde{U}_1\delta_{i1} + \tilde{U}_2\delta_{i2}}{4}(2\ln(1-s^2) - 4\ln\epsilon + \tilde{\kappa}_1 s) + O(\varepsilon\tilde{\boldsymbol{\kappa}},\varepsilon). \tag{3.9}$$

Substituting (3.9) into (2.25) allows us to compute the components of the hydrodynamic force density as

$$\bar{f}_1 = 2\pi\tilde{U}_1\tilde{\eta}_s\left[-\frac{1}{\ln\varepsilon}+\frac{1}{2(\ln\varepsilon)^2}\left(1-2\ln 2-\ln\left(\frac{1-s^2}{\tilde{\lambda}^2}\right)-s\,\frac{\tilde{\kappa}_1}{2}\right)\right] + O((\ln\varepsilon)^{-3}, \tilde{\boldsymbol{\kappa}}\varepsilon(\ln\varepsilon)^{-1}), \tag{3.10}$$

$$\bar{f}_2 = 2\pi\tilde{U}_2\tilde{\eta}_s\left[-\frac{2}{\ln\varepsilon}+\frac{1}{(\ln\varepsilon)^2}\left(-1-2\ln 2-\ln\left(\frac{1-s^2}{\tilde{\lambda}^2}\right)-s\,\frac{\tilde{\kappa}_1}{2}\right)\right] + O((\ln\varepsilon)^{-3}, \tilde{\boldsymbol{\kappa}}\varepsilon(\ln\varepsilon)^{-1}). \tag{3.11}$$

Evaluating the total force and torque in (2.26) and (2.27) requires integrating terms containing $\tilde{\eta}_s(s) = 1 + s\tilde{\kappa}_1/2$. Writing the total force $\boldsymbol{F}$ and torque $\boldsymbol{T}$ as asymptotic expansions, we have

$$F_i = F_i^{(0)} + \tilde{\kappa}_1 F_i^{(1)} + O(\tilde{\kappa}_1^2, \varepsilon\tilde{\kappa}_2, \varepsilon\tilde{\kappa}_3), \tag{3.12}$$

$$T_i = T_i^{(0)} + \tilde{\kappa}_1 T_i^{(1)} + O(\tilde{\kappa}_1^2, \varepsilon\tilde{\kappa}_2, \varepsilon\tilde{\kappa}_3). \tag{3.13}$$

The terms proportional to U_1 are, to leading order in $O((\ln\varepsilon)^{-2})$, given by

$$F_1^{(0)} = a\eta_0 U_1\left[\frac{4\pi}{\ln(2a/b)+C_1}\right], \quad C_1 = -\frac{1}{2}+\frac{1}{4}\int_{-1}^{1}\ln\left(\frac{1-s^2}{\tilde{\lambda}^2}\right)\mathrm{d}s, \tag{3.14}$$

$$F_1^{(1)} = a\eta_0 U_1\left[-\frac{\pi}{2(\ln(b/a))^2}\int_{-1}^{1} s\ln\left(\frac{1-s^2}{\tilde{\lambda}^2}\right)\mathrm{d}s\right], \tag{3.15}$$

$$T_2^{(0)} = 0, \tag{3.16}$$

$$T_2^{(1)} = 0, \tag{3.17}$$

while the terms proportional to U_2 are, to leading order in $O((\ln\varepsilon)^{-2})$, given by

$$F_2^{(0)} = a\eta_0 U_2\left[\frac{8\pi}{\ln(2a/b)+C_2}\right], \quad C_2 = \frac{1}{2}+\frac{1}{4}\int_{-1}^{1}\ln\left(\frac{1-s^2}{\tilde{\lambda}^2}\right)\mathrm{d}s, \tag{3.18}$$

$$F_2^{(1)} = a\eta_0 U_2\left[-\frac{\pi}{(\ln(b/a)^2}\int_{-1}^{1} s\ln\left(\frac{1-s^2}{\tilde{\lambda}^2}\right)\mathrm{d}s\right], \tag{3.19}$$

$$T_3^{(0)} = a\eta_0 U_2\left[-\frac{2\pi}{(\ln(b/a))^2}\int_{-1}^{1} s^2\ln\left(\frac{1-s^2}{\tilde{\lambda}^2}\right)\mathrm{d}s\right], \tag{3.20}$$

$$T_3^{(1)} = a^2\eta_0 U_2\left[\frac{4\pi}{3(\ln(2a/b)+C_3)}\right], \quad C_3 = 1+\frac{3}{4}\int_{-1}^{1} s^2\ln\left(\frac{1-s^2}{\tilde{\lambda}^2}\right)\mathrm{d}s. \tag{3.21}$$

Note that in the dimensional calculations above, and in all dimensional expressions to come, we have replaced $\ln\varepsilon$ by $\ln(b/a)$, so that the geometrical parameters appear explicitly.

From our results, we see that if the dimensionless cross-section shape $\tilde{\lambda}(s)$ is symmetric about its centre $s = 0$, then $F_1^{(1)}$, $F_2^{(1)}$ and $T_3^{(0)}$ are all zero. Therefore, $\tilde{\kappa}_1$ does not affect the force $\boldsymbol{F}$ to leading order. For T_3, however, there is now a leading-order correction

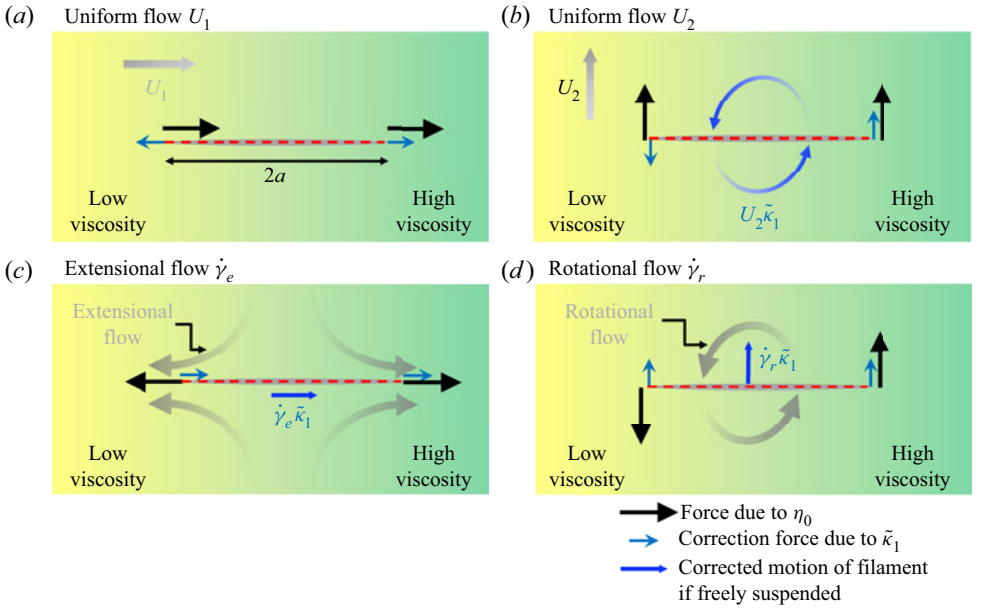

Figure 2. Illustration of the leading-order effect on the hydrodynamic forces applied to a filament held fixed in a prescribed (*a*,*b*) uniform, and (*c*,*d*) linear flow field. We use (grey) bold arrows to represent the external flow, and thin arrows to represent the force density applied to the fixed filament; thin black arrows are the forces (or motion) for a filament in a uniform viscosity field, while thin blue arrows illustrate the correction due to the linear viscosity gradient, which induces new forces and torques.

proportional to $\tilde{\kappa}_1$. If the particle was freely suspended in the linear flow field $U_2\hat{\boldsymbol{e}}_2$ at an orientation $R(s) = s\hat{\boldsymbol{e}}_1$, then this result is equivalent to the filament slowly rotating with an angular velocity $\boldsymbol{\omega} \cdot \hat{\boldsymbol{e}}_3 \propto U_2\tilde{\kappa}_1$.

3.1.2. *Discussion and physical interpretation*

We now provide a physical interpretation for this induced torque (and thus the rotation) due to a gradient in viscosity, which we illustrate in figures 2(*a*,*b*). A filament held fixed in a uniform (prescribed) flow field with constant viscosity gradient $\tilde{\kappa}_1$ experiences a greater hydrodynamic force density $\bar{\boldsymbol{f}}$ in the region where the viscosity is larger than η_0, and a decrease in $\bar{\boldsymbol{f}}$ in the region where the viscosity is smaller. We use arrows in figures 2(*a*,*b*) to illustrate this change in $\bar{\boldsymbol{f}}$: the black (thin) arrows correspond to $\bar{\boldsymbol{f}}$ generated in the constant-viscosity case (η_0), while the blue (thin) arrows show the additional $\bar{\boldsymbol{f}}$ induced by a gradient of viscosity $\tilde{\kappa}_1$. For symmetric shapes with $\tilde{\lambda}(-s) = \tilde{\lambda}(s)$, the effect of $\tilde{\kappa}_1$ on $\bar{\boldsymbol{f}}$ is to thus create an antisymmetric distribution about the centre $s = 0$, as a difference with the symmetric distribution arising in the case of a constant viscosity η_0. The antisymmetric distribution of $\bar{\boldsymbol{f}}$ results in no torque at leading order when the flow is aligned with the filament (figure 2*a*), but an applied torque proportional to $\tilde{\kappa}_1$ when the uniform flow is perpendicular to the filament (figure 2*b*). Note that when $\bar{\boldsymbol{f}}$ is proportional to $\hat{\boldsymbol{e}}_1$, the leading torque distribution is of order $O(\varepsilon^2)$ (Cox 1971) and is thus subdominant in our leading expansion with respect to ε. If the filament was torque- and force-free, then instead of net forces and torques, the viscosity gradient $\tilde{\kappa}_1$ results in an additional rotational or translational motion, as illustrated by the (thick) blue arrows in figure 2.

3.2. *Linear flow field*

After the case of a uniform flow, we now assume that the filament is held fixed in a linear external flow field, consisting of an extensional flow $\dot{\gamma}_e(x_1\hat{\boldsymbol{e}}_1 - (x_2/2)\hat{\boldsymbol{e}}_2 - (x_3/2)\hat{\boldsymbol{e}}_3)$ and a rotational flow $\dot{\gamma}_r(-x_2\hat{\boldsymbol{e}}_1 + x_1\hat{\boldsymbol{e}}_2)$.

3.2.1. *Computation of forces and torques*

Non-dimensionalising $\dot{\gamma}_e$ and $\dot{\gamma}_r$ by a typical shear scale $\dot{\gamma}$, (2.24) becomes

$$J_i = \frac{\tilde{\eta}_s}{4}\left[\int_{-1}^{s-\epsilon} + \int_{s+\epsilon}^{1}\right] \tilde{G}^V_{ij}\left(s-\hat{s},0,0\right)\left(\tilde{\dot{\gamma}}_e\delta_{j1} + 2\tilde{\dot{\gamma}}_r\delta_{j2}\right) s\,\mathrm{d}\hat{s}. \tag{3.22}$$

Evaluating the integral in (3.22) analytically, one finds to leading order

$$J_i = \frac{\tilde{\dot{\gamma}}_e\delta_{i1} + \tilde{\dot{\gamma}}_r\delta_{i2}}{2}\left(s\left(\ln(1-s^2) - 2 - 2\ln\epsilon\right) + \frac{\tilde{\kappa}_1}{4}\left(s^2-1\right)\right) + O(\varepsilon\tilde{\boldsymbol{\kappa}},\varepsilon). \tag{3.23}$$

Substituting J_i into (2.25) gives

$$\begin{aligned}\bar{f}_1 = {}& \tilde{\dot{\gamma}}_e\pi\left[-\frac{2s}{\ln\varepsilon} + \frac{s}{(\ln\varepsilon)^2}\left(3 - 2\ln 2 - \ln\left(\frac{1-s^2}{\tilde{\lambda}^2}\right)\right)\right] \\ & + \tilde{\dot{\gamma}}_e\pi\tilde{\kappa}_1\left[-\frac{s^2}{\ln\varepsilon} + \frac{1}{4(\ln\varepsilon)^2}\left(1 + s^2\left(5 - 4\ln 2 - 2\ln\left(\frac{1-s^2}{\tilde{\lambda}^2}\right)\right)\right)\right] \\ & + O((\ln\varepsilon)^{-3}, \tilde{\boldsymbol{\kappa}}\varepsilon/\ln\varepsilon),\end{aligned} \tag{3.24}$$

$$\begin{aligned}\bar{f}_2 = {}& \tilde{\dot{\gamma}}_r\pi\left[-\frac{2s}{\ln\varepsilon} + \frac{s}{(\ln\varepsilon)^2}\left(1 - 2\ln 2 - \ln\left(\frac{1-s^2}{\tilde{\lambda}^2}\right)\right)\right] \\ & + \pi\dot{\gamma}_r\tilde{\kappa}_1\left[-\frac{s^2}{\ln\varepsilon} + \frac{1}{2(\ln\varepsilon)^2}\left(1 + s^2\left(1 - 4\ln 2 - 2\ln\left(\frac{1-s^2}{\tilde{\lambda}^2}\right)\right)\right)\right] \\ & + O((\ln\varepsilon)^{-3}, \tilde{\boldsymbol{\kappa}}\varepsilon/\ln\varepsilon).\end{aligned} \tag{3.25}$$

We may then use $\bar{\boldsymbol{f}}$ to evaluate the leading-order contribution to $\boldsymbol{F}$ in (2.26), T_3 in (2.27), and the stresslet S_{11} in (2.28), while all other components of $\boldsymbol{T}$ and $\boldsymbol{S}$ are zero to leading order in ε. At leading order in the viscosity gradient $\tilde{\boldsymbol{\kappa}}$, one finds

$$F_i \approx F_i^{(0)} + \tilde{\kappa}_1 F_i^{(1)}, \quad T_3 \approx T_3^{(0)} + \tilde{\kappa}_1 T_3^{(1)}, \quad S_{11} \approx S_{11}^{(0)} + \tilde{\kappa}_1 S_{11}^{(1)}. \tag{3.26a–c}$$

In the extensional flow field, the leading terms proportional to the extension rate $\dot{\gamma}_e$ are, to leading order in $O((\ln\varepsilon)^{-2})$, given by

$$F_1^{e(0)} = a^2\eta_0\dot{\gamma}_e\left[-\frac{\pi}{(\ln(b/a))^2}\int_{-1}^{1} s\ln\left(\frac{1-s^2}{\tilde{\lambda}^2}\right)\mathrm{d}s\right], \tag{3.27}$$

$$F_1^{e(1)} = a^2\eta_0\dot{\gamma}_e\left[\frac{2\pi}{3(\ln(2a/b)+C_{e_1})}\right], \quad C_{e_1} = -2+\frac{3}{4}\int_{-1}^{1} s^2\ln\left(\frac{1-s^2}{\tilde{\lambda}^2}\right)\mathrm{d}s, \tag{3.28}$$

$$S_{11}^{e(0)} = a^3\eta_0\dot{\gamma}_e\left[-\frac{4\pi}{3(\ln(2a/b)+C_{e_2})}\right], \quad C_{e_2} = -\frac{3}{2}+\frac{3}{4}\int_{-1}^{1} s^2\ln\left(\frac{1-s^2}{\tilde{\lambda}^2}\right)\mathrm{d}s, \tag{3.29}$$

$$S_{11}^{e(1)} = a^3\eta_0\dot{\gamma}_e\left[\frac{\pi}{2(\ln(b/a))^2}\int_{-1}^{1} s^3\ln\left(\frac{1-s^2}{\tilde{\lambda}^2}\right)\mathrm{d}s\right]. \tag{3.30}$$

Similarly, in the rotational flow field, the leading terms proportional to the rotation rate $\dot{\gamma}_r$ are given by

$$F_2^{r(0)} = a^2\eta_0\dot{\gamma}_r\left[-\frac{2\pi}{(\ln(b/a))^2}\int_{-1}^{1} s\ln\left(\frac{1-s^2}{\tilde{\lambda}^2}\right)\mathrm{d}s\right], \tag{3.31}$$

$$F_2^{r(1)} = a^2\eta_0\dot{\gamma}_r\left[\frac{4\pi}{3(\ln(2a/b)+C_{r_1})}\right], \quad C_{r_1} = -1+\frac{3}{4}\int_{-1}^{1} s^2\ln\left(\frac{1-s^2}{\tilde{\lambda}^2}\right)\mathrm{d}s, \tag{3.32}$$

$$T_3^{r(0)} = a^3\eta_0\dot{\gamma}_r\left[\frac{8\pi}{3(\ln(2a/b)+C_{r_2})}\right], \quad C_{r_2} = -\frac{1}{2}+\frac{3}{4}\int_{-1}^{1} s^2\ln\left(\frac{1-s^2}{\tilde{\lambda}^2}\right)\mathrm{d}s, \tag{3.33}$$

$$T_3^{r(1)} = a^3\eta_0\dot{\gamma}_r\left[-\frac{\pi}{(\ln(b/a))^2}\int_{-1}^{1} s^3\ln\left(\frac{1-s^2}{\tilde{\lambda}^2}\right)\mathrm{d}s\right]. \tag{3.34}$$

Here, the superscripts e and r have been added to highlight the contribution to $\boldsymbol{F}$, T_3 and S_{11} from the extensional ($\dot{\gamma}_e$) and rotational ($\dot{\gamma}_r$) flow fields, respectively.

3.2.2. *Discussion and physical interpretation*

Here also, if the cross-sectional shape $\tilde{\lambda}(s)$ is symmetric about the centre $s = 0$, then $F_1^{e(0)}$, $S_{11}^{e(1)}$, $F_2^{r(0)}$ and $T_3^{r(1)}$ are all zero. Therefore, the presence of a viscosity gradient induces a force acting on the filament proportional to $\tilde{\kappa}_1(\dot{\gamma}_e\hat{\boldsymbol{e}}_1 + \dot{\gamma}_r\hat{\boldsymbol{e}}_2)$. If the particle was freely suspended, then this result is equivalent to there being a small drift velocity proportional to $\dot{\gamma}_e\hat{\boldsymbol{e}}_1 + \dot{\gamma}_r\hat{\boldsymbol{e}}_2$, as illustrated for both the rotational flow in figure 2(*c*) and the extensional flow in figure 2(*d*). Similar to the case of a uniform flow field, the effect of $\tilde{\kappa}_1$ on a filament with $\tilde{\lambda}(-s) = \tilde{\lambda}(s)$ held fixed in a linear flow field is to induce an additional symmetric contribution to $\bar{\boldsymbol{f}}$, compared to the antisymmetric contribution in a constant viscosity η_0. The components of $\bar{\boldsymbol{f}}$ due to η_0 and $\tilde{\kappa}_1$ are sketched in figure 2 with black and blue arrows, respectively. The new symmetric contribution of $\bar{\boldsymbol{f}}$ creates a new force due to $\tilde{\kappa}_1$ given to leading order in (3.28) and (3.32).

3.3. *Sedimentation*

The linearity of the incompressible Stokes equations leads to a set of linear relationships between the stress, and therefore the force and torque, exerted on a fixed body and the rotational and translational motion of a freely suspended body in an external linear flow field, with the linear coefficient being referred to as the 'resistance coefficient' (Kim & Karrila 2013). The leading force, torques and stress given in (3.14)–(3.21) and

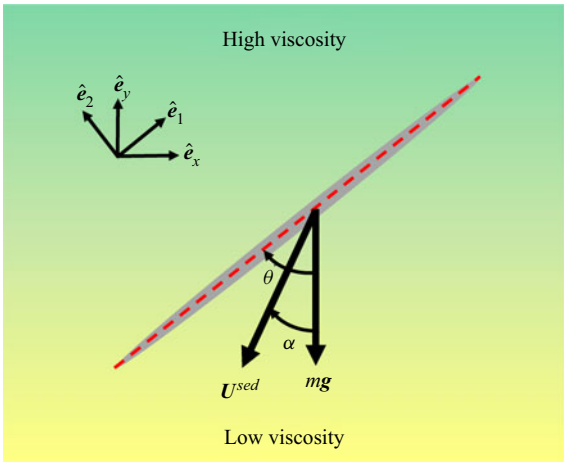

Figure 3. Sketch of a filament settling under the action of gravity (side view); the filament is oriented at an angle θ from the vertical and sediments instantaneously at angle α to the vertical.

(3.27)–(3.34) can be used to obtain the leading resistance coefficients acting on the filament. Assuming a symmetric cross-section with $\tilde{\lambda}(-s) = \tilde{\lambda}(s)$, we have

$$\lambda_1 = F_1^{(0)}/U_1, \quad \lambda_2 = F_2^{(0)}/U_2, \quad \lambda_r = \tilde{\kappa}_1 F_2^{r(1)}/\dot{\gamma}_r \tag{3.35a–c}$$

and

$$L_2 = \tilde{\kappa}_1 T_3^{(1)}/U_2, \quad L_r = T_3^{r(0)}/\dot{\gamma}_r, \tag{3.36a,b}$$

where $F_1^{(0)}$, $F_2^{(0)}$, $T_3^{(1)}$, $F_2^{r(1)}$ and $T_3^{r(0)}$ are given in (3.14), (3.18), (3.21), (3.32) and (3.33), respectively.

We can now use these resistance coefficients to examine the sedimentation of a straight filament under the action of gravity. This set-up is illustrated in figure 3. The lab frame is set in a Cartesian coordinate system spanned by the unit vectors $(\hat{\boldsymbol{e}}_x, \hat{\boldsymbol{e}}_y, \hat{\boldsymbol{e}}_3)$. We assume that the filament is aligned at an angle θ from the gravitational field, has weight $-mg\hat{\boldsymbol{e}}_y$, and is settling with an orientation α from the vertical. The fluid has a constant viscosity gradient, which, in the lab frame, is set as $\tilde{\boldsymbol{\kappa}} = \tilde{\kappa}_x\hat{\boldsymbol{e}}_x + \tilde{\kappa}_y\hat{\boldsymbol{e}}_y$ so that the dynamics occurs in the $(\hat{\boldsymbol{e}}_x, \hat{\boldsymbol{e}}_y)$ plane. In a constant viscosity field, a filament settles without rotating and with a uniform drift orientation given by $\tan\alpha = (\lambda_1/\lambda_2)\tan\theta$ (Taylor 1967; Guyon *et al.* 2015).

In the case of a viscosity gradient, the sedimentation velocity $\boldsymbol{U}^{sed}$ and the angular velocity $\Omega^{sed}\hat{\boldsymbol{e}}_3$ are found by balancing the hydrodynamic forces with gravity, and by applying the zero-torque condition, as appropriate for a freely suspended filament. The resulting balances are written in the body frame along the three basis vectors

$$\hat{\boldsymbol{e}}_1: \quad mg\cos\theta + \tilde{\lambda}_1 U_1^{sed} = 0, \tag{3.37}$$

$$\hat{\boldsymbol{e}}_2: \quad mg\sin\theta + \tilde{\lambda}_2 U_2^{sed} + \tilde{\lambda}_r \Omega^{sed} = 0, \tag{3.38}$$

$$\hat{\boldsymbol{e}}_3: \quad L_r\Omega^{sed} + L_2 U_2^{sed} = 0. \tag{3.39}$$

Solving (3.37)–(3.39) to leading order in $\tilde{\kappa}_1$ and in $\ln(a/b)$ in the lab frame gives

$$\Omega^{sed} = \frac{mg}{16\pi a^2\eta}\ln\left(\frac{a}{b}\right)\left(\tilde{\kappa}_x\sin\theta + \tilde{\kappa}_y\cos\theta\right)\sin\theta, \tag{3.40}$$

$$U_x^{sed} = -\frac{mg}{8\pi a\eta}\ln\left(\frac{a}{b}\right)\cos\theta\sin\theta, \tag{3.41}$$

$$U_y^{sed} = -\frac{mg}{8\pi a\eta}\ln\left(\frac{a}{b}\right)(1+\cos^2\theta). \tag{3.42}$$

We see that the impact of the viscosity gradient $\tilde{\boldsymbol{\kappa}}$ is to create a non-zero angular rotation Ω^{sed} (which is therefore zero in the case of a constant viscosity). We further observe that $\Omega^{sed} = 0$ at a critical angle for which $\tan\theta_c = -\tilde{\kappa}_y/\tilde{\kappa}_x$. It is straightforward to show that θ_c is stable if and only if $\tilde{\kappa}_1$ acts in the direction opposite to the gravitational field (i.e. if $\tilde{\kappa}_y > 0$). Indeed, for θ_c to be stable, we need $(\mathrm{d}\Omega^{sed}/\mathrm{d}\theta)|_{\theta=\theta_c} < 0$. But

$$\frac{\mathrm{d}\Omega^{sed}}{\mathrm{d}\theta} = \frac{mg}{16\pi a^2\eta}\ln\left(\frac{a}{b}\right)\cos^2\theta(\tilde{\kappa}_x\tan\theta + \tilde{\kappa}_y(1-\tan^2\theta)). \tag{3.43}$$

Evaluating this expression at $\theta = \theta_c$ gives

$$\left.\frac{\mathrm{d}\Omega^{sed}}{\mathrm{d}\theta}\right|_{\theta=\theta_c} = -\frac{mg}{16\pi a^2\eta}\ln\left(\frac{a}{b}\right)\cos^2\theta_c\left(1+\frac{\tilde{\kappa}_y^2}{\tilde{\kappa}_x^2}\right)\tilde{\kappa}_y, \tag{3.44}$$

which is negative if and only if $\tilde{\kappa}_y > 0$.

3.3.1. *Filament orientation*

The effect of the viscosity gradient $\tilde{\boldsymbol{\kappa}}$ on θ can be shown explicitly by integrating (3.40) to obtain the angle $\theta(t)$. With an initial condition $\theta_0 \equiv \theta(0)$, we obtain

$$\theta(t) = \begin{cases} \operatorname{acot}\left(\cot\theta_0 + K\tilde{\kappa}_x t\right), & K = -\dfrac{mg}{a^2\eta}\dfrac{\ln(a/b)}{16\pi}, \quad \text{if } \tilde{\kappa}_y = 0, \\ \operatorname{atan2}\left(\tilde{\kappa}_y, \left(\dfrac{\tilde{\kappa}_y}{\tan\theta_0} + \tilde{\kappa}_x\right)\exp\left(K\tilde{\kappa}_y t\right) - \tilde{\kappa}_x\right), & \text{otherwise.} \end{cases} \tag{3.45}$$

Here, we have introduced the two-argument arc-tangent function $\operatorname{atan2}(x, y)$, which returns the angle of the complex number $x + iy$. Note that the prefactor K is the contribution to $mgL_2/(\tilde{\kappa}_1(L_2\lambda_r - L_r\lambda_2))$ at leading order in $\ln(\varepsilon)$ and $\tilde{\kappa}_1$.

With the result in (3.45), we see that as $t \to \infty$, the exponential in (3.45) vanishes if and only if $\tilde{\kappa}_y > 0$ and thus $\theta \to \theta_c$, as predicted above; otherwise, $\theta \to \pi$ or $\theta \to 0$. We illustrate an example of the orientation dynamics in figure 4 using the parameters $\tilde{\kappa}_x = -\tilde{\kappa}_y = 0.01$ (solid black line) and $\tilde{\kappa}_x = \tilde{\kappa}_y = 0.01$ (dashed red line), and an initial condition $\theta_0 = \pi/2$. For $\tilde{\kappa}_y = -0.01$, $\theta_c = -\tilde{\kappa}_y/\tilde{\kappa}_x \equiv \pi/4$ is unstable. For all values of $\theta_0 \neq \theta_c$, the filament always rotates away from θ_c to align itself in the direction of gravity. This is seen in figure 4, where as $t \to \infty$, the filament rotates away from θ_c towards $\theta = \pi$. For $\tilde{\kappa}_y = 0.01$, however, $\theta_c = 3\pi/4$ is stable. Therefore, $\theta \to \theta_c$ as $t \to \infty$ for all initial orientations.

If $\tilde{\kappa}_x = 0$ and $\tilde{\kappa}_y > 0$, then the filament always rotates towards $\theta = \pi/2$, regardless of its initial condition, thus aligning perpendicular to the gravitational field with time. Otherwise, for $\tilde{\kappa}_y < 0$, the filament rotates in the opposite direction, towards $\theta = 0$ for $0 \leq \theta_0 < \pi/2$, or towards $\theta = \pi$ for $\pi/2 < \theta_0 \leq \pi$, thus aligning in the direction of

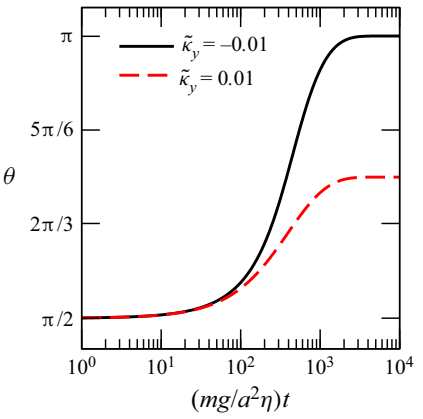

Figure 4. Rotation of a settling filament with aspect ratio $b/a = 10^{-4}$ under a constant viscosity gradient with $\tilde{\kappa}_x = 0.01$, and $\tilde{\kappa}_y = 0.01$ (dashed red line) or $\tilde{\kappa}_y = -0.01$ (solid black line), as predicted by (3.45).

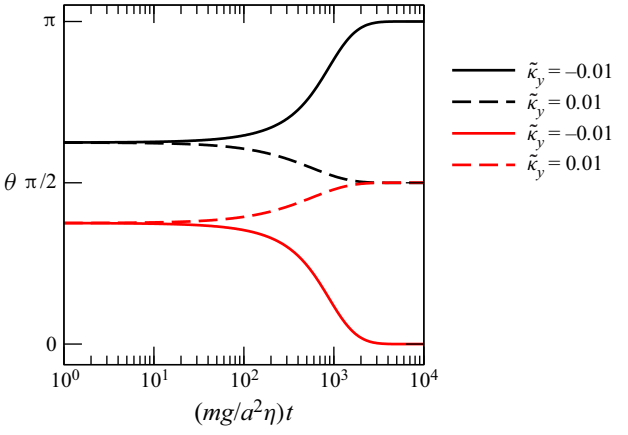

Figure 5. Rotation of a filament settling under the action of gravity in a viscosity gradient with $\tilde{\kappa}_x = 0$, and $\tilde{\kappa}_y = 0.01$ (dashed lines) and $\tilde{\kappa}_y = -0.01$ (solid lines), for $\theta_0 = 5\pi/8$ (black lines) and $\theta_0 = 3\pi/8$ (red lines), as predicted by (3.45).

gravity with time. An example of this rotation for $\theta_0 = 5\pi/8, 3\pi/8$ and $\tilde{\kappa}_y = \pm 1$ is illustrated in figure 5.

If $\theta_0 = \pi/2$, then the sign of $\tilde{\kappa}_x$ determines in which direction the particle rotates: if $\tilde{\kappa}_x > 0$, then the particle rotates towards θ_c or $\theta = \pi$; otherwise, θ decreases towards θ_c or $\theta = 0$. An example of this dependency is shown in figure 6 for $\tilde{\kappa}_y = 0$ and $\tilde{\kappa}_x = \pm 0.01$. For $\tilde{\kappa}_x = 0.01$, $\theta(t) \to \pi$, and for $\tilde{\kappa}_x = -0.01$, $\theta(t) \to 0$, as expected.

3.3.2. *Drift orientation*

We focus next on the drift of the filament. Denoting by $x(t)$ and $y(t)$ the time-varying coordinates of the filament, the drift orientation angle α is the solution to $\tan\alpha = x(t)/y(t)$. To find α, we can solve (3.41)–(3.42) explicitly to compute the trajectory of the filament. Two cases have to be considered separately, depending on the value of $\tilde{\kappa}_y$.

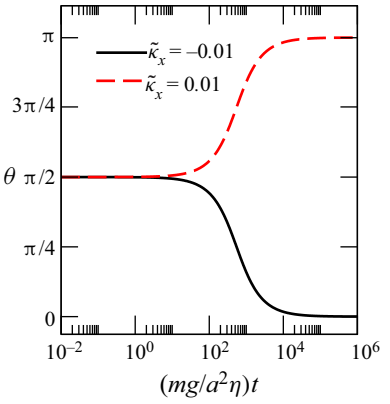

Figure 6. Rotation of a filament settling under the action of gravity in a viscosity gradient with $\tilde{\kappa}_y = 0$, and $\tilde{\kappa}_x = 0.01$ (dashed red line) and $\tilde{\kappa}_x = -0.01$ (solid black line), as predicted by (3.45). (The filament has aspect ratio $b/a = 10^{-4}$.)

When $\tilde{\kappa}_y \neq 0$, we obtain to leading order in $\tilde{\boldsymbol{\kappa}}$ and $\ln \varepsilon$ the trajectory

$$x(t) - x(0) = -4\,\frac{\tilde{\kappa}_x \tilde{\kappa}_y Ka}{\tilde{\kappa}_x{}^2 + \tilde{\kappa}_y^2}\,t + \frac{a}{\tilde{\kappa}_x^2 + \tilde{\kappa}_y^2}\left(2\tilde{\kappa}_y\left(\arctan(K_2) - \pi/2 + \theta_0\right) + \tilde{\kappa}_x \ln(K_1)\right), \tag{3.46}$$

$$y(t) - y(0) = \frac{2(2\tilde{\kappa}_x^2 + \tilde{\kappa}_y^2)Ka}{\tilde{\kappa}_x^2 + \tilde{\kappa}_y^2}\,t + \frac{a}{\tilde{\kappa}_x^2 + \tilde{\kappa}_y^2}\left(2\tilde{\kappa}_x\left(\pi/2 - \theta_0 - \arctan(K_2)\right) + \tilde{\kappa}_y \ln(K_1)\right), \tag{3.47}$$

where

$$K_1 = \frac{\left(\tilde{\kappa}_x \tan\theta_0 + \tilde{\kappa}_y\right)^2 \mathrm{e}^{2K\tilde{\kappa}_y t} - 2\left((\tan\theta_0)^2\,\tilde{\kappa}_x^2 + \tilde{\kappa}_x\tilde{\kappa}_y \tan\theta_0\right)\mathrm{e}^{K\tilde{\kappa}_y t}}{\tilde{\kappa}_y^2\left((\tan\theta_0)^2 + 1\right)} + \frac{(\tan\theta_0)^2(\tilde{\kappa}_x^2 + \tilde{\kappa}_y^2)}{\tilde{\kappa}_y^2\left((\tan\theta_0)^2 + 1\right)}, \tag{3.48}$$

$$K_2 = \frac{\mathrm{e}^{K\tilde{\kappa}_y t}\,\tilde{\kappa}_x \sin\theta_0 + \mathrm{e}^{K\tilde{\kappa}_y t}\,\tilde{\kappa}_y \cos\theta_0 - \tilde{\kappa}_x \sin\theta_0}{\sin\theta_0\,\tilde{\kappa}_y}. \tag{3.49}$$

As $t \to \infty$, the displacement of the filament tends to the limit behaviour

$$x(t) - x(0) \approx \begin{cases} \dfrac{\tilde{\kappa}_x \tilde{\kappa}_y mg}{4\pi(\tilde{\kappa}_x^2 + \tilde{\kappa}_y^2)\eta a} \ln\left(\dfrac{a}{b}\right) t + b_x, & \text{if } \tilde{\kappa}_y > 0, \\ \dfrac{a\left(\tilde{\kappa}_y\left(\pi\,\mathrm{sign}\left(\dfrac{\tilde{\kappa}_x}{\tilde{\kappa}_y} + \cot\theta_0\right) - \dfrac{\pi}{2} + \theta_0\right) + \tilde{\kappa}_x K_4\right)}{2(\tilde{\kappa}_x^2 + \tilde{\kappa}_y^2)}, & \text{if } \tilde{\kappa}_y < 0, \end{cases} \tag{3.50}$$

$$y(t)-y(0)\approx\begin{cases}-\dfrac{(2\tilde{\kappa}_x^2+\tilde{\kappa}_y^2)mg}{8\pi(\tilde{\kappa}_x^2+\tilde{\kappa}_y^2)\eta a}\ln\left(\dfrac{a}{b}\right)t+b_y, & \text{if } \tilde{\kappa}_y>0,\\ -\dfrac{3\,mg}{8\pi\eta a}\ln\left(\dfrac{a}{b}\right)t+c_y, & \text{if } \tilde{\kappa}_y<0,\end{cases}\tag{3.51}$$

where

$$b_x=\frac{a\left(2\tilde{\kappa}_y\left(\theta_0-\arctan\left(\dfrac{\tilde{\kappa}_x}{\tilde{\kappa}_y}\right)-\dfrac{\pi}{2}\right)+\tilde{\kappa}_xK_3\right)}{2(\tilde{\kappa}_x^2+\tilde{\kappa}_y^2)},\tag{3.52}$$

$$b_y=\frac{a\left(2\tilde{\kappa}_x\left(\dfrac{\pi}{2}-\theta_0+\arctan\left(\dfrac{\tilde{\kappa}_x}{\tilde{\kappa}_y}\right)\right)+\tilde{\kappa}_yK_3\right)}{2(\tilde{\kappa}_x^2+\tilde{\kappa}_y^2)},\tag{3.53}$$

$$c_y=\frac{a\left(2\tilde{\kappa}_x\left(\dfrac{\pi}{2}-\theta_0-\dfrac{\pi}{2}\,\mathrm{sign}\left(\dfrac{\tilde{\kappa}_x}{\tilde{\kappa}_y}+\cot\theta_0\right)\right)+\tilde{\kappa}_yK_4\right)}{2(\tilde{\kappa}_x^2+\tilde{\kappa}_y^2)}\tag{3.54}$$

and

$$K_3=\ln\left(\frac{(\tilde{\kappa}_x{}^2+\tilde{\kappa}_y{}^2)(\tan\theta_0)^2}{\tilde{\kappa}_y{}^2\left((\tan\theta_0)^2+1\right)}\right),\quad K_4=\ln\left(\frac{\left(\tilde{\kappa}_x\tan\theta_0+\tilde{\kappa}_y\right)^2}{\tilde{\kappa}_y{}^2\left((\tan\theta_0)^2+1\right)}\right).\tag{3.55a,b}$$

The drift orientation angle α simplifies considerably in the limit $t\to\infty$, and it is seen to depend on the sign of $\tilde{\kappa}_y$. If the viscosity gradient acts in the direction opposite to the gravitational field ($\tilde{\kappa}_y>0$, viscosity decreasing with depth), then both $x(t)$ and $y(t)$ vary linearly with t as $t\to\infty$: the displacements of $x(t)$ and $y(t)$ are of the form a_it+b_i as $t\to\infty$, where a_i and b_i are constants for $i=x,y$, respectively. The ratio between the linear coefficients, a_x/a_y, is then used to determine the limit value $\alpha\to\alpha_c$ as $t\to\infty$ as

$$\tan\alpha_c=\lim_{t\to\infty}\tan\alpha=\frac{a_x}{a_y}\equiv-\frac{2\tilde{\kappa}_x\tilde{\kappa}_y}{\tilde{\kappa}_y^2+2\tilde{\kappa}_x^2}.\tag{3.56}$$

In the long-time limit $t\to\infty$, the filament tends therefore towards a steady state where it translates with a fixed deflection angle α_c. This asymptotic result is reminiscent of the uniform viscosity behaviour where the filament does not rotate and sediments at a constant deflection angle whose value is set by the filament orientation. The maximum deflection angle, in that case, has magnitude $\alpha\approx19.5^\circ$ obtained for $\theta\approx54.7^\circ$ in the case of an asymptotically slender filament (Taylor 1967; Guyon *et al.* 2015). The crucial difference brought to the viscosity gradient is that now the values of θ_c and α_c can be tuned by varying the ratio $\tilde{\kappa}_y/\tilde{\kappa}_x$.

If now $\tilde{\kappa}_y<0$ (i.e. when the viscosity increases with depth), then as $t\to\infty$, the filament aligns in the direction parallel to the gravitational field and it falls vertically. As a result, the filament drifts over a finite amount in the $\hat{\boldsymbol{e}}_x$ direction with a drift orientation $\alpha\propto1/t$ as $t\to\infty$. The total drift displacement in the $\hat{\boldsymbol{e}}_x$ direction, given in (3.50), depends on the time required for the filament to reorientate parallel to the gravitational field, which depends on $\tilde{\kappa}_x$, $\tilde{\kappa}_y$ and θ_0. This result is similar to the sedimentation of a ribbon torus (Koens & Lauga 2017), which also reorientates in a direction parallel to the gravitational field. For the case of the ribbon, the total drift in the $\hat{\boldsymbol{e}}_x$ direction depends on the angle

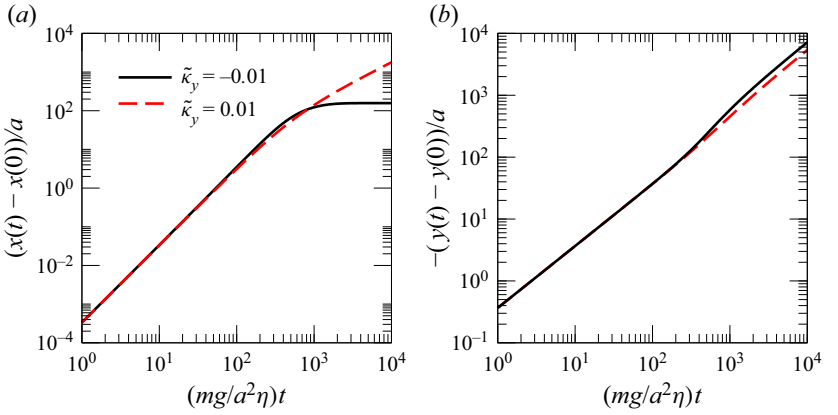

Figure 7. Displacement (a, b) of the filament in figure 4 settling under a constant viscosity gradient with $\tilde{\kappa}_x = 0.01$, and $\tilde{\kappa}_y = 0.01$ (dashed red line) or $\tilde{\kappa}_y = -0.01$ (solid black line), as predicted by (3.46) and (3.47).

between the plane of the ribbon and its centreline normal vector, whereas here the total drift of the filament depends on the imposed viscosity gradient $\tilde{\boldsymbol{\kappa}}$.

We illustrate in figures 7(*a*,*b*) examples of the two different types of trajectories obtained as a function of the sign of $\tilde{\kappa}_y$; animated versions of the long-time behaviour are provided in the supplementary material (movies 1 and 2) available at https://doi.org/10.1017/jfm.2023.336. After sufficient time, we see that when $\tilde{\kappa}_y = -0.01$, $x(t)$ tends to a constant and $y(t)$ varies linearly with time (solid black line), whereas both $x(t)$ and $y(t)$ vary linearly with time for $\tilde{\kappa}_y = 0.01$ (dashed red line), in agreement with the theory. At small time, in comparison, the trajectories are almost identical for $\tilde{\kappa}_y = -0.01$ and $\tilde{\kappa}_y = 0.01$. This result is because the trajectories depend on the orientation of the filament to leading order, which is identical for these given examples in the limit $t \to 0$.

We note that a different solution exists in the special limit where $\tilde{\kappa}_y = 0$, i.e. when the gradient in viscosity is purely horizontal. In that case, the displacement of the filament is given to leading order in $\tilde{\boldsymbol{\kappa}}$ and $\ln \varepsilon$ by

$$x(t) - x(0) = \frac{a \ln\left(\left|K^2 \tilde{\kappa}_x^2 t^2 \left(1 - \cos^2\theta_0\right) + 2Kt\tilde{\kappa}_x \cos\theta_0 \sin\theta_0 + 1\right|\right)}{\tilde{\kappa}_x}, \tag{3.57}$$

$$y(t) - y(0) = -\frac{mg}{4\pi\eta a} \ln\left(\frac{a}{b}\right) t - \frac{a\left(2 \arctan\left(\cot\theta_0 + tK\tilde{\kappa}_x\right) - 2\theta_0 + \pi\right)}{\tilde{\kappa}_x}. \tag{3.58}$$

As $t \to \infty$, this displacement tends to

$$x(t) - x(0) = \frac{a \ln(t)}{\tilde{\kappa}_x} + \frac{a \ln\left(\left|K^2 \tilde{\kappa}_x^2 \left(1 - \cos^2\theta_0\right)\right|\right)}{\tilde{\kappa}_x}, \tag{3.59}$$

$$y(t) - y(0) = -\frac{mg}{4\pi\eta a} \ln\left(\frac{a}{b}\right) t - \frac{a}{\tilde{\kappa}_x}\left(\pi - \pi \operatorname{sign}(\tilde{\kappa}_x) - 2\theta_0\right). \tag{3.60}$$

If $\theta_0 = 0$ or $\theta_0 = \pi$, then the filament falls vertically without drifting in the $\hat{\boldsymbol{e}}_x$ direction. Otherwise, as $t \to \infty$, the filament slowly drifts in the $\hat{\boldsymbol{e}}_x$ direction with a drift proportional to $\ln(t)/\tilde{\kappa}_x$. Therefore, the deflection angle varies as $\alpha \propto \ln(t)/t$, which slowly decays to zero as $t \to \infty$. Examples of the displacement for $\tilde{\kappa}_x = \pm 0.01$ are shown in figures 8(*a*,*b*), with an animated version of the long-time behaviour provided in the supplementary

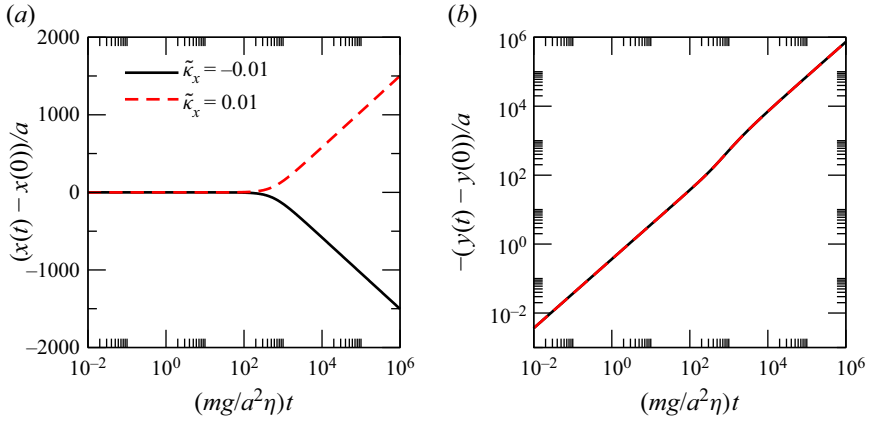

Figure 8. Displacement (a, b) of the filament in figure 6 settling under the action of gravity in a viscosity gradient with $\tilde{\kappa}_y = 0$, and $\tilde{\kappa}_x = 0.01$ (dashed red line) and $\tilde{\kappa}_x = -0.01$ (solid black line), as predicted by (3.57) and (3.58).

material (movie 3 for $\tilde{\kappa}_x = 0.01$). At long time, $y(t) - y(0)$ is the same for both $\tilde{\kappa}_x = \pm 0.01$ since the linear term in $y(t)$ is independent of $\tilde{\kappa}_x$ to leading order.

4. Toroidal filament in a linear viscosity gradient

4.1. *Uniform flow field*

After the straight configuration, we now consider the case of a toroidal filament of uniform cross-section ($\tilde{\lambda}(s) = 1$) held fixed in a linear flow field $\boldsymbol{u}^\infty = U_1\hat{\boldsymbol{e}}_1 + U_2\hat{\boldsymbol{e}}_2$ in a fluid with a constant viscosity gradient $\tilde{\boldsymbol{\kappa}}$. The (dimensionless) centreline of the toroidal filament is parametrised in polar coordinates as $\tilde{\boldsymbol{R}}(\theta) = \cos\theta\,\hat{\boldsymbol{e}}_1 + \sin\theta\,\hat{\boldsymbol{e}}_3$ for $s = \theta \in [\theta_0, \theta_0 + 2\pi]$. Using this notation and dimensionalising U_1 and U_2 by a typical speed U, (2.24) becomes

$$J_1 = \lim_{\epsilon\to 0} \frac{\tilde{U}_1\tilde{\eta}_s}{4} \int_{\theta+\epsilon}^{\theta+2\pi-\epsilon} [(2 - \sin^2\hat{\theta})\tilde{G}^V_{11}(x_1', 0, x_3') + \sin\hat{\theta}\cos\hat{\theta}\,\tilde{G}^V_{13}(x_1', 0, x_3')]\mathrm{d}\hat{\theta}, \tag{4.1}$$

$$J_2 = \lim_{\epsilon\to 0} \frac{\tilde{U}_2\tilde{\eta}_s}{2} \int_{\theta+\epsilon}^{\theta+2\pi-\epsilon} \tilde{G}^V_{22}\left(x_1', 0, x_3'\right)\mathrm{d}\hat{\theta}, \tag{4.2}$$

$$J_3 = \lim_{\epsilon\to 0} \frac{\tilde{U}_1\tilde{\eta}_s}{4} \int_{\theta+\epsilon}^{\theta+2\pi-\epsilon} [(2 - \sin^2\hat{\theta})\tilde{G}^V_{13}\left(x_1', 0, x_3'\right) + \sin\hat{\theta}\cos\hat{\theta}\,\tilde{G}^V_{33}\left(x_1', 0, x_3'\right)]\mathrm{d}\hat{\theta}, \tag{4.3}$$

with

$$x_1' = \cos\theta - \cos\hat{\theta}, \quad x_3' = \sin\theta - \sin\hat{\theta}. \tag{4.4a,b}$$

Evaluating these integrals analytically to leading order in $\tilde{\boldsymbol{\kappa}}$ and ε gives

$$J_1 = \tilde{U}_1\left[\tfrac{1}{2}\sin^2\theta - \ln\epsilon + 2\ln 2 + \tfrac{2}{3}\tilde{\kappa}_1\cos\theta + \tfrac{1}{2}\tilde{\kappa}_3\sin\theta\right] + O(\varepsilon\tilde{\boldsymbol{\kappa}}, \varepsilon), \tag{4.5}$$

$$J_2 = \tilde{U}_2\left[2\ln 2 - \ln\epsilon + \tfrac{1}{2}\left(\tilde{\kappa}_1\cos\theta + \tilde{\kappa}_3\sin\theta\right)\right] + O(\varepsilon\tilde{\boldsymbol{\kappa}}, \varepsilon), \tag{4.6}$$

$$J_3 = \tilde{U}_1\left[-\frac{\sin(2\theta)}{4} + \frac{1}{2}\tilde{\kappa}_1\sin\theta - \frac{1}{3}\tilde{\kappa}_3\cos\theta\right] + O(\varepsilon\tilde{\boldsymbol{\kappa}}, \varepsilon). \tag{4.7}$$

Substituting (4.5)–(4.7) into (2.25) allows us to compute the dimensionless force density components

$$\bar{f}_1 = 2\pi\tilde{U}_1\tilde{\eta}_s\left[\frac{A}{\ln\varepsilon} + \frac{B}{(\ln\varepsilon)^2} + O((\ln\varepsilon)^{-3}, \tilde{\boldsymbol{\kappa}}\varepsilon(\ln\varepsilon)^{-1})\right], \tag{4.8}$$

$$\bar{f}_2 = 2\pi\tilde{U}_2\tilde{\eta}_s\left[\frac{-2}{\ln\varepsilon} - \frac{6\ln 2 + \tilde{\kappa}_1\cos\theta + \tilde{\kappa}_3\sin\theta}{(\ln\varepsilon)^2}\right] + O((\ln\varepsilon)^{-3}, \tilde{\boldsymbol{\kappa}}\varepsilon(\ln\varepsilon)^{-1}), \tag{4.9}$$

with

$$A = \left(1 + \tfrac{1}{2}\left(\tilde{\kappa}_1\cos\theta + \tilde{\kappa}_3\sin\theta\right)\right)(\sin^2\theta - 2), \tag{4.10}$$

$$B = -\tfrac{1}{2}\left(1 + \tfrac{1}{2}\left(\tilde{\kappa}_1\cos\theta + \tilde{\kappa}_3\sin\theta\right)\right)(9\ln 2 + 1 + \cos(2\theta) + 3\ln 2\cos(2\theta)) - \tfrac{1}{24}\left(\tilde{\kappa}_3(\sin(3\theta) + 13\sin\theta) + \tilde{\kappa}_1(\cos(3\theta) + 31\cos\theta)\right). \tag{4.11}$$

The results for the net force and torque $\boldsymbol{F}$ and $\boldsymbol{T}$ (in dimensional form), written in increasing order of $\tilde{\boldsymbol{\kappa}}$, are

$$F_i = F_i^{(0)} + F_i^{(1)} + \cdots, \quad T_i = T_i^{(0)} + T_i^{(1)} + \cdots. \tag{4.12a,b}$$

The terms proportional to U_1, up to order $O((\ln\varepsilon)^{-2})$, are given by

$$F_1^{(0)} = a\eta_0 U_1\left[\frac{6\pi^2}{\ln(2\pi a/b) + C_{T1}}\right], \quad C_{T1} = \frac{1}{3} - \ln\left(\frac{\pi}{4}\right), \tag{4.13}$$

$$F_1^{(1)} = 0, \tag{4.14}$$

$$T_2^{(0)} = 0, \tag{4.15}$$

$$T_2^{(1)} = \tilde{\kappa}_3 a^2\eta_0 U_1\left[\frac{5\pi^2}{4\left(\ln(2\pi a/b) + C_{T2}\right)}\right], \quad C_{T2} = \frac{16}{15} - \ln\left(\frac{\pi}{4}\right), \tag{4.16}$$

while those proportional to U_2, up to order $O((\ln\varepsilon)^{-2})$, are written as

$$F_2^{(0)} = a\eta_0 U_2\left[\frac{8\pi^2}{\ln(2\pi a/b) + C_{T3}}\right], \quad C_{T3} = -\ln\left(\frac{\pi}{4}\right) + \frac{1}{2}, \tag{4.17}$$

$$F_2^{(1)} = 0, \tag{4.18}$$

$$T_3^{(0)}/\tilde{\kappa}_1 = -T_1^{(0)}/\tilde{\kappa}_3 = 0, \tag{4.19}$$

$$T_3^{(1)}/\tilde{\kappa}_1 = -T_1^{(1)}/\tilde{\kappa}_3 = a^2\eta_0 U_2\left[\frac{2\pi^2}{\ln(2\pi a/b) + C_{T4}}\right], \quad C_{T4} = \frac{3}{2} - \ln\left(\frac{\pi}{4}\right). \tag{4.20}$$

Similar to the straight filament, we see that the leading-order effect of the viscosity gradient is to exert a torque on the toroidal filament proportional to either $\tilde{\kappa}_1$ or $\tilde{\kappa}_3$.

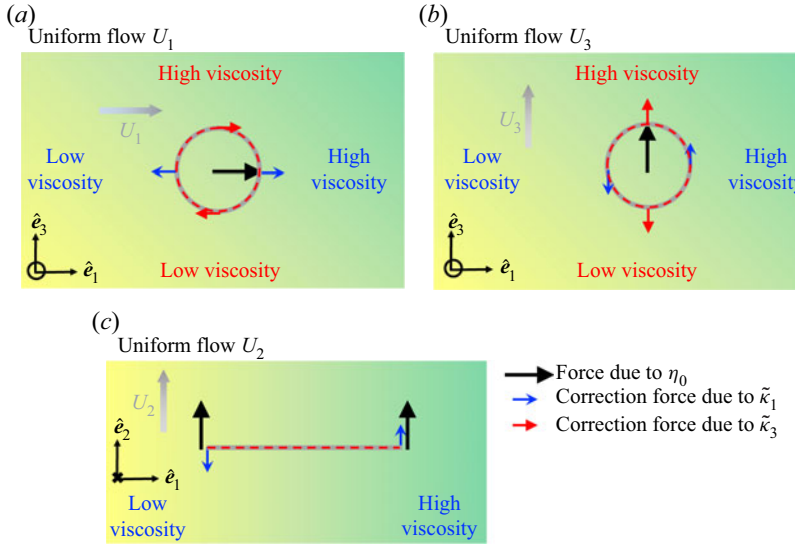

Figure 9. Sketch of the leading force distribution applied to a toroidal filament held fixed in a uniform flow field at selected orientations. The bold (grey) arrows represent the flow field, and the thin arrows represent the force density due to this flow field. Black (thin) arrows are the leading forces due to η_0, and the blue and red arrows show the corrections due to $\tilde{\kappa}_1$ and $\tilde{\kappa}_3$, respectively.

By symmetry of the toroidal filament, the leading torque due to a uniform flow $U_3\hat{\boldsymbol{e}}_3$ is equal to $-T_2^{(1)}U_3\tilde{\kappa}_1/(U_1\tilde{\kappa}_3)$, where $T_2^{(1)}$ is given in (4.16).

In figure 9, we provide sketches to illustrate the effect of a viscosity gradient $\tilde{\boldsymbol{\kappa}}$ on the force and torques exerted on the toroidal filament. The viscosity gradient leads to an antisymmetric force density $\bar{\boldsymbol{f}}$, creating a viscous torque. The direction of this torque acts either in the tangential direction of the surface of the toroidal filament or in the normal direction to the plane in which the toroidal filament lies.

4.2. *Rotational flow field*

We now assume that the external flow $\boldsymbol{u}^\infty$ is rotational. Specifically, we write it as the sum of two rotational flows $\dot{\gamma}_3(-x_2\hat{\boldsymbol{e}}_1 + x_1\hat{\boldsymbol{e}}_2)$ and $\dot{\gamma}_2(-x_3\hat{\boldsymbol{e}}_1 + x_1\hat{\boldsymbol{e}}_3)$. Non-dimensionalising $\dot{\gamma}_1$ and $\dot{\gamma}_2$ by a shear scale $\dot{\gamma}$, (2.24) becomes

$$J_1 = \lim_{\epsilon\to 0}\frac{\tilde{\dot{\gamma}}_2\tilde{\eta}_s}{4}\int_{\theta+\epsilon}^{\theta+2\pi-\epsilon}\tilde{G}^V_{11}\left(x_1',0,x_3'\right)\left(\cos^2\hat{\theta}\sin\hat{\theta}-\sin\hat{\theta}(2-\sin^2\hat{\theta})\right)$$
$$+\tilde{G}^V_{13}\left(x_1',0,x_3'\right)\left(\cos\hat{\theta}(2-\cos^2\hat{\theta})-\cos\hat{\theta}\sin^2\hat{\theta}\right)\mathrm{d}\hat{\theta}, \tag{4.21}$$

$$J_2 = \lim_{\epsilon\to 0}\frac{\tilde{\dot{\gamma}}_3\tilde{\eta}_s}{2}\int_{\theta+\epsilon}^{\theta+2\pi-\epsilon}\tilde{G}^V_{22}\left(x_1',0,x_3'\right)\mathrm{d}\hat{\theta}, \tag{4.22}$$

$$J_3 = \lim_{\epsilon\to 0}\frac{\tilde{\dot{\gamma}}_2\tilde{\eta}_s}{4}\int_{\theta+\epsilon}^{\theta+2\pi-\epsilon}\tilde{G}^V_{33}\left(x_1',0,x_3'\right)\left(\cos\hat{\theta}(2-\cos^2\hat{\theta})-\cos\hat{\theta}\sin^2\hat{\theta}\right)$$
$$+\tilde{G}^V_{31}\left(x_1',0,x_3'\right)\left(\cos^2\hat{\theta}\sin\hat{\theta}-\sin\hat{\theta}(2-\sin^2\hat{\theta})\right)\mathrm{d}\hat{\theta}. \tag{4.23}$$

To leading order in $\tilde{\boldsymbol{\kappa}}$, one then finds

$$J_1 = \tilde{\dot{\gamma}}_2\left[-\sin\theta\left(2\ln 2 - \tfrac{3}{2} - \ln\epsilon\right) + \tfrac{1}{6}\left(\tilde{\kappa}_3\cos 2\theta - \tilde{\kappa}_1\sin 2\theta\right)\right], \tag{4.24}$$

$$J_2 = \tilde{\dot{\gamma}}_3\left[\cos\theta\left(2\ln 2 - 2 - \ln\epsilon\right) + \tfrac{1}{12}\left(\tilde{\kappa}_1(\cos 2\theta - 3) + \tilde{\kappa}_3\sin 2\theta\right)\right], \tag{4.25}$$

$$J_3 = \tilde{\dot{\gamma}}_2\left[\cos\theta\left(2\ln 2 - \tfrac{3}{2} - \ln\epsilon\right) + \tfrac{1}{6}\left(\tilde{\kappa}_1\cos 2\theta + \tilde{\kappa}_3\sin 2\theta\right)\right]. \tag{4.26}$$

Substituting the expressions for J_i into (2.25) gives, to leading order in $\tilde{\kappa}_1$, the force density with components

$$\bar{f}_i = 2\pi\tilde{\eta}_s(\tilde{\dot{\gamma}}_2(\delta_{i1} + \delta_{i3}) + \tilde{\dot{\gamma}}_3\delta_{i2})\left[\frac{A_i}{\ln\varepsilon} + \frac{B_i}{(\ln\varepsilon)^2} + O((\ln\varepsilon)^{-3}, \tilde{\boldsymbol{\kappa}}\varepsilon(\ln\varepsilon)^{-1})\right], \tag{4.27}$$

for $i = 1$, 2 and 3, with constants given by

$$A_1 = -\sin\theta(\sin^2\theta - 2) - \sin\theta\cos^2\theta, \tag{4.28}$$

$$B_1 = B_{11}(\sin^2\theta - 2) - B_{12}\sin\theta\cos\theta - \tfrac{1}{2}\sin\theta, \tag{4.29}$$

$$A_2 = -2\cos\theta, \tag{4.30}$$

$$B_2 = 3\cos\theta\,(1 - 2\ln 2) + \tfrac{1}{6}\left(\tilde{\kappa}_1(3 - \cos 2\theta) - \tilde{\kappa}_3\sin 2\theta\right), \tag{4.31}$$

$$A_3 = \cos\theta(\cos^2\theta - 2) + \sin^2\theta\cos\theta, \tag{4.32}$$

$$B_3 = B_{12}(\cos^2\theta - 2) - B_{11}\sin\theta\cos\theta - \tfrac{1}{2}\cos\theta, \tag{4.33}$$

$$B_{11} = -\tfrac{3}{2}\sin\theta\,(2\ln 2 - 1) + \tfrac{1}{6}\left(\tilde{\kappa}_3\cos 2\theta - \tilde{\kappa}_1\sin 2\theta\right), \tag{4.34}$$

$$B_{11} = \tfrac{3}{2}\cos\theta\,(2\ln 2 - 1) + \tfrac{1}{6}\left(\tilde{\kappa}_1\cos 2\theta + \tilde{\kappa}_3\sin 2\theta\right). \tag{4.35}$$

The results for $\boldsymbol{F}$ and $\boldsymbol{T}$ (in dimensional form), in increasing order of $\tilde{\boldsymbol{\kappa}}$, are

$$F_i = F_i^{(0)} + F_i^{(1)} + \cdots, \quad T_i = T_i^{(0)} + T_i^{(1)} + \cdots. \tag{4.36a,b}$$

The terms proportional to $\dot{\gamma}_3$ are, to leading order $O((\ln\varepsilon)^{-2})$, given by

$$F_2^{\dot{\gamma}_3(0)} = 0, \tag{4.37}$$

$$F_2^{\dot{\gamma}_3(1)} = a^2\eta_0\dot{\gamma}_3\tilde{\kappa}_1\left[\frac{2\pi^2}{\ln(2\pi a/b) + C_{T5}}\right], \quad C_{T5} = -\frac{5}{2} - \ln\left(\frac{\pi}{4}\right), \tag{4.38}$$

$$T_3^{\dot{\gamma}_3(0)} = a^3\eta_0\dot{\gamma}_3\left[\frac{4\pi^2}{\ln(2\pi a/b) + C_{T6}}\right], \quad C_{T6} = -\frac{3}{2} - \ln\left(\frac{\pi}{4}\right), \tag{4.39}$$

$$T_3^{\dot{\gamma}_3(1)} = 0. \tag{4.40}$$

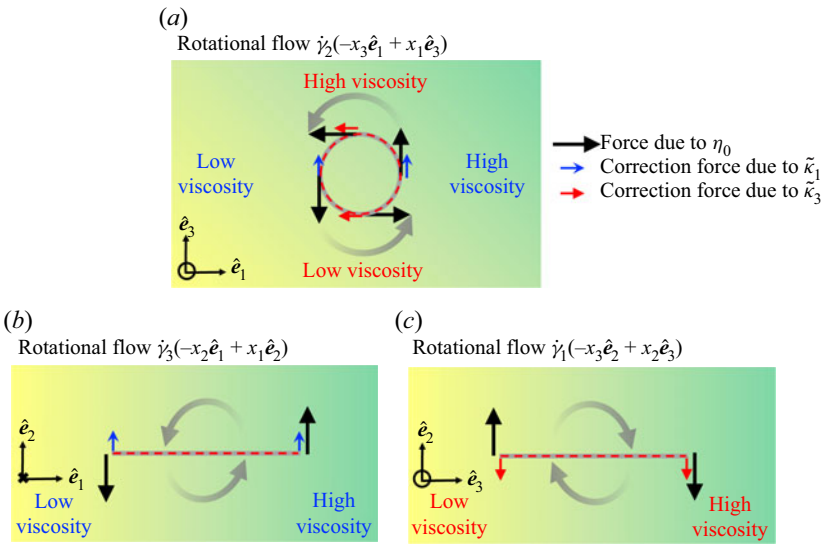

Figure 10. Sketch of the leading force and torque applied to a toroidal filament held fixed in a rotational flow field. The thin arrows represent the force density, and the bolder (grey) arrows represent the external flow field. Black (thin) arrows are the leading hydrodynamic forces due to a constant viscosity η_0, and the blue and red (thin) arrows represent the force corrections due to the gradients $\tilde{\kappa}_1$ and $\tilde{\kappa}_3$, respectively.

Similarly, the terms proportional to $\dot{\gamma}_2$ are, to leading order $O((\ln\varepsilon)^{-2})$, given by

$$F_1^{\dot{\gamma}_2(0)} = 0, \tag{4.41}$$

$$F_1^{\dot{\gamma}_2(1)} = -a^2\eta_0\dot{\gamma}_2\tilde{\kappa}_3\left[\frac{\pi^2}{\ln(2\pi a/b) + C_{T7}}\right], \quad C_{T7} = -\frac{7}{3} - \ln\left(\frac{\pi}{4}\right), \tag{4.42}$$

$$F_3^{\dot{\gamma}_2}/\tilde{\kappa}_1 = -F_1^{\dot{\gamma}_2}/\tilde{\kappa}_3, \tag{4.43}$$

$$T_2^{\dot{\gamma}_2(0)} = a^3\eta_0\dot{\gamma}_2\left[\frac{4\pi^2}{\ln(2\pi a/b) + C_{T6}}\right], \quad C_{T6} = -2 - \ln\left(\frac{\pi}{4}\right), \tag{4.44}$$

$$T_2^{\dot{\gamma}_2(1)} = 0. \tag{4.45}$$

Here, the superscripts $(\,)^{\dot{\gamma}_3}$ and $()^{\dot{\gamma}_2}$ have been added to highlight the contributions to $\boldsymbol{F}$ and $\boldsymbol{T}$ from the rotational flow fields proportional to $\dot{\gamma}_3$ and $\dot{\gamma}_2$, respectively. Similar to the straight filament, the effect of $\tilde{\boldsymbol{\kappa}}$ is to create a leading force acting on the toroidal filament proportional to $-\dot{\gamma}_2\tilde{\kappa}_3\hat{\boldsymbol{e}}_x + \dot{\gamma}_3\tilde{\kappa}_1\hat{\boldsymbol{e}}_y + \dot{\gamma}_2\tilde{\kappa}_1\hat{\boldsymbol{e}}_z$. A sketch is provided in figure 10 to illustrate this effect. A new symmetric contribution to $\bar{\boldsymbol{f}}$ is induced by $\tilde{\boldsymbol{\kappa}}$. In addition, by symmetry of the toroidal filament for $\boldsymbol{u}^\infty = \dot{\gamma}_1(-x_2\hat{\boldsymbol{e}}_3 + x_3\hat{\boldsymbol{e}}_2)$, one obtains $F_2^{\dot{\gamma}_1}/(\dot{\gamma}_1\tilde{\kappa}_3) = -F_2^{\dot{\gamma}_3}/(\dot{\gamma}_3\tilde{\kappa}_1)$.

4.3. *Sedimentation*

We finally consider the sedimentation dynamics of the toroidal filament. If we constrain the motion of the settling filament in the $(\hat{\boldsymbol{e}}_x, \hat{\boldsymbol{e}}_y)$ plane, then its governing equations are the same as in (3.37)–(3.38) but with $\tilde{\lambda}_1, \tilde{\lambda}_2, \tilde{\lambda}_r, L_2, L_r$ interchanged for the equivalent resistance coefficients for the toroidal geometry. At leading order in $\ln(a/b)$, the velocity

of the settling toroidal filament becomes then

$$\Omega^{sed} = \frac{mg}{16\pi a^2\eta}\ln\left(\frac{a}{b}\right)\left(\tilde{\kappa}_x\sin\theta + \tilde{\kappa}_y\cos\theta\right)\sin\theta, \tag{4.46}$$

$$U_x^{sed} = -\frac{mg}{24\pi a\eta}\ln\left(\frac{a}{b}\right)\cos\theta\sin\theta, \tag{4.47}$$

$$U_y^{sed} = -\frac{mg}{24\pi a\eta}\ln\left(\frac{a}{b}\right)(3+\cos^2\theta). \tag{4.48}$$

We see that the velocity of the toroidal filament is similar to that of the settling straight filament (see (3.40)–(3.42)), up to a change in prefactors. Therefore, $\theta(t)$ is the same as that given in (3.45) but with K becoming the toroidal value K^T given by

$$K^T = -\frac{mg}{a^2\eta}\frac{\ln(a/b)}{16\pi}. \tag{4.49}$$

Similarly to the case of a straight filament, if there exists a viscosity gradient in the direction opposite to the gravitational field, then the toroidal filament aligns at an angle with $\tan\theta_c = -\tilde{\kappa}_y/\tilde{\kappa}_x$ as $t\to\infty$. Otherwise, it aligns in the direction of the gravitational field itself. Moreover, for an initial orientation $\theta_0 = \pi/2$, the direction at which the filament rotates depends on the sign of $\tilde{\kappa}_x$: a toroidal filament has a positive angular velocity if $\tilde{\kappa}_x > 0$, causing it to rotate towards $\theta\to\pi$, and a negative angular velocity if $\tilde{\kappa}_x < 0$, inducing rotation in the opposite direction towards $\theta\to 0$.

The difference with the straight filament lies in the direction and speed at which the toroidal filament settles. In the limit $t\to\infty$, one finds explicitly

$$x(t)-x(0) \approx \begin{cases} \dfrac{\tilde{\kappa}_x\tilde{\kappa}_y mg}{12\pi(\tilde{\kappa}_x^2+\tilde{\kappa}_y^2)\eta a}\ln\left(\dfrac{a}{b}\right)t + b_x^T, & \text{if } \tilde{\kappa}_y > 0, \\ \dfrac{a\left(\tilde{\kappa}_y\left(\pi\,\mathrm{sign}\left(\dfrac{\tilde{\kappa}_x}{\tilde{\kappa}_y}+\cot\theta_0\right)-\dfrac{\pi}{2}+\theta_0\right)+\tilde{\kappa}_x K_4\right)}{3(\tilde{\kappa}_x^2+\tilde{\kappa}_y^2)}, & \text{if } \tilde{\kappa}_y < 0, \end{cases} \tag{4.50}$$

$$y(t)-y(0) \approx \begin{cases} -\dfrac{(4\tilde{\kappa}_x^2+3\tilde{\kappa}_y^2)mg}{24\pi(\tilde{\kappa}_x^2+\tilde{\kappa}_y^2)\eta a}\ln\left(\dfrac{a}{b}\right)t + b_y^T, & \text{if } \tilde{\kappa}_y > 0, \\ -\dfrac{mg}{6\pi\eta a}\ln\left(\dfrac{a}{b}\right)t + c_y^T, & \text{if } \tilde{\kappa}_y < 0, \end{cases} \tag{4.51}$$

where

$$b_x^T = \frac{a\left(2\tilde{\kappa}_y\left(\theta_0 - \arctan\left(\dfrac{\tilde{\kappa}_x}{\tilde{\kappa}_y}\right)-\dfrac{\pi}{2}\right)+\tilde{\kappa}_x K_3\right)}{3(\tilde{\kappa}_x^2+\tilde{\kappa}_y^2)}, \tag{4.52}$$

$$b_y^T = \frac{a\left(2\tilde{\kappa}_x\left(\dfrac{\pi}{2}-\theta_0+\arctan\left(\dfrac{\tilde{\kappa}_x}{\tilde{\kappa}_y}\right)\right)+\tilde{\kappa}_y K_3\right)}{3(\tilde{\kappa}_x^2+\tilde{\kappa}_y^2)}, \tag{4.53}$$

$$c_y^T = \frac{3a\left(2\tilde{\kappa}_x\left(\dfrac{\pi}{2}-\theta_0-\dfrac{\pi}{2}\mathrm{sign}\left(\dfrac{\tilde{\kappa}_x}{\tilde{\kappa}_y}+\cot\theta_0\right)\right)+\tilde{\kappa}_y K_4\right)}{\tilde{\kappa}_x^2+\tilde{\kappa}_y^2}, \tag{4.54}$$

with the coefficients K_3 and K_4 defined in (3.51).

Therefore, when $\tilde{\kappa}_y > 0$, the toroidal filament drifts with an orientation

$$\lim_{t\to\infty} \tan\alpha \approx \frac{-2\tilde{\kappa}_x\tilde{\kappa}_y}{3\tilde{\kappa}_x^2 + 4\tilde{\kappa}_y^2}. \tag{4.55}$$

If instead $\tilde{\kappa}_y < 0$, then the toroidal filament drifts a finite amount in the $\hat{\boldsymbol{e}}_x$ direction until it becomes aligned in the direction of the gravitational force, where it falls without any drift in the $\hat{\boldsymbol{e}}_x$ direction; the size of the drift is given in (4.50). Here, the total drift in the $\hat{\boldsymbol{e}}_x$ direction for the toroidal filament is $2/3$ of the equivalent drift for a straight filament.

Note that the displacements given in (4.50) and (4.51) are not valid in the singular case where $\tilde{\kappa}_y = 0$. In this case, the displacement of the toroidal filament is obtained as

$$x(t) - x(0) = \frac{a\ln\left(\left|(K^T)^2\tilde{\kappa}_x^2 t^2(1-\cos^2\theta_0) + 2K^T t\tilde{\kappa}_x\cos\theta_0\sin\theta_0 + 1\right|\right)}{3\tilde{\kappa}_x}, \tag{4.56}$$

$$y(t) - y(0) = -\frac{mg}{6\pi\eta a}\ln\left(\frac{a}{b}\right)t - \frac{a\left(2\arctan\left(\cot\theta_0 + tK^T\tilde{\kappa}_x\right) - 2\theta_0 + \pi\right)}{3\tilde{\kappa}_x}. \tag{4.57}$$

As $t\to\infty$, this displacement tends to

$$x(t) - x(0) = \frac{2a\ln(t)}{3\tilde{\kappa}_x} + \frac{a\ln\left(\left|(K^T)^2\tilde{\kappa}_x^2(1-\cos^2\theta_0)\right|\right)}{3\tilde{\kappa}_x}, \tag{4.58}$$

$$y(t) - y(0) = -\frac{mg}{6\pi\eta a}\ln\left(\frac{a}{b}\right)t - \frac{a}{3\tilde{\kappa}_x}\left(\pi - \pi\,\mathrm{sign}(\tilde{\kappa}_x) - 2\theta_0\right). \tag{4.59}$$

Again, we see that the finite drift of the toroidal filament in both the $\hat{\boldsymbol{e}}_x$ and $\hat{\boldsymbol{e}}_y$ directions is $2/3$ of that obtained for a straight filament.

5. Discussion

In this paper, motivated by recent biophysical studies on the motion of active particles and organisms in fluids with heterogeneous viscosity fields, we addressed the dynamics of slender filaments in a fluid with linearly varying viscosity. Specifically, we derived the leading-order correction to resistive-force theory (RFT) due to a small viscosity gradient in the limit $\varepsilon \ll |\tilde{\boldsymbol{\kappa}}| \ll 1$, where ε is the aspect ratio of the slender filament, and $\tilde{\boldsymbol{\kappa}}$ is the dimensionless gradient in viscosity. The leading-order solution to the force density $\boldsymbol{f}$ over the arc length s of the slender body is identical to the classical RFT (Cox 1970) up to the local viscosity coefficient (which now contains a uniform viscosity gradient) and the integrand vector '$\boldsymbol{J}$', which corresponds to the integrand of a line distribution of point forces over $R(s)$ in the corresponding viscosity gradient flow field.

We have then used the modified RFT to evaluate the leading effects of $\tilde{\boldsymbol{\kappa}}$ on the force and torques applied to (i) a slender filament and (ii) a toroidal filament held fixed in uniform and rotational flow fields. The effect of $\tilde{\boldsymbol{\kappa}}$ on the filament is to increase f_i/U_i^∞ in the region of higher viscosity, and decrease f_i/U_i^∞ in the lower region of viscosity, thus creating generically an antisymmetric contribution to f_i/U_i^∞. The magnitude and direction of the antisymmetric contribution of f_i/U_i^∞ are proportional to $\tilde{\kappa}_1$, i.e. the direction of the viscosity gradient parallel to $R(s)$. As a result, a filament in a uniform flow field $\boldsymbol{U}^\infty = U_1\hat{\boldsymbol{e}}_1 + U_2\hat{\boldsymbol{e}}_2$ experiences a torque $T\hat{\boldsymbol{e}}_3 \propto \tilde{\kappa}_1 U_2$, and a filament in a rotational or extensional flow field $\boldsymbol{U}^\infty = \dot{\gamma}_e x_1\hat{\boldsymbol{e}}_1 + \dot{\gamma}_r x_1\hat{\boldsymbol{e}}_2$ experiences a force $\boldsymbol{F} \propto \dot{\gamma}_e\tilde{\kappa}_1\hat{\boldsymbol{e}}_1 + \dot{\gamma}_r\tilde{\kappa}_1\hat{\boldsymbol{e}}_2$. The effect of $\tilde{\boldsymbol{\kappa}}$ on the toroidal filament held fixed in the $(\hat{\boldsymbol{e}}_1, \hat{\boldsymbol{e}}_3)$ plane is similar to

the straight filament, except that the toroidal filament experiences leading effects from a viscosity gradient in both the $\hat{\boldsymbol{e}}_1$ and $\hat{\boldsymbol{e}}_3$ directions. For example, a toroidal filament held fixed in a uniform flow field (U_1, U_2, U_3) experiences a leading torque $T_3/\tilde{\kappa}_1 = -T_1/\tilde{\kappa}_3 \propto U_2$ and $T_2 \propto \tilde{\kappa}_3 U_1 - \tilde{\kappa}_1 U_3$.

Finally, we have used our results for the force and torque distributions acting on the straight and toroidal filaments to estimate their trajectories under the action of gravity when their sedimentation is confined to the $(\hat{\boldsymbol{e}}_x, \hat{\boldsymbol{e}}_y)$ plane. We found that the effects of a viscosity gradient on both filaments are similar: $\tilde{\boldsymbol{\kappa}}$ causes the straight body to rotate with an angular velocity proportional to $\tilde{\kappa}_1$, or proportional to either $\tilde{\kappa}_1$ or $\tilde{\kappa}_3$ for the torus. The effect of $\tilde{\boldsymbol{\kappa}}$ in the direction parallel to the gravitational field $-g\hat{\boldsymbol{e}}_y$ is as follows. Suppose that $\tilde{\kappa}_y$ is directed in the direction opposite to the gravitational field. In that case, the filaments rotate towards a stable orientation $\tan\theta_c = -\tilde{\kappa}_y/\tilde{\kappa}_x$, where they drift at a finite angle α that depends on $\tilde{\kappa}_y$, $\tilde{\kappa}_x$ and the shape of the slender body. Otherwise, the filaments rotate to align parallel to the gravitational field. For a filament initially aligned perpendicular to the gravitational force field, the direction of rotation depends on $\tilde{\kappa}_x$, and the rate of rotation depends on both $\tilde{\kappa}_x$ and the shape of the slender body.

The impact of a viscosity gradient can be compared to the classical dynamics of a filament in a uniform viscosity field. In that case, a straight filament settles without rotating and with a maximum drift orientation $\alpha_c \approx -19.5^\circ$ obtained for the critical orientation $\theta_c \approx -54.7^\circ$ (Taylor 1967; Guyon *et al.* 2015). This result is similar to what we obtained for the long-time motion of both the straight and toroidal filaments when $\tilde{\kappa}_y$ acts in the direction opposite to the gravitational field. The difference is that now the values of the α_c and θ_c can be tuned by varying the components $\tilde{\kappa}_x$ and $\tilde{\kappa}_y$ of the viscosity gradient. These results suggest that viscosity gradients provide a new means to control the drift and orientation of slender particles in flow without having to tune their shape (Koens & Lauga 2017). Note that since the angular velocity of the filaments scales with the viscosity gradient, in the limit of weak gradient considered theoretically here, the time scales for reorientation are asymptotically large. Further numerical and experimental work will be needed to characterise how sharp gradients in viscosity affect the motion of slender bodies.

Beyond the dynamics of passive filaments addressed in this paper, we expect our results to be relevant to the transport of active particles in complex fluids (Li, Lauga & Ardekani 2021). Recent studies have reported experimentally the manner in which heterogeneous viscosity fields affect the locomotion of flagellated algal swimmers (Coppola & Kantsler 2021; Stehnach *et al.* 2021) or cells with slender shapes (Takabe *et al.* 2017). The theoretical predictions in this paper will enable future work to characterise how the waving motion, or rotation, of slender filaments is affected by local changes in viscosity, thereby enabling the study of locomotion in fluids with heterogeneous viscosity fields.

Supplementary movies. Supplementary movies are available at https://doi.org/10.1017/jfm.2023.336.

Funding. Funding from the Stokes Research Fellowship, Pembroke College, Cambridge is gratefully acknowledged (C.K.). This project has also received funding from the European Research Council (ERC) under the European Union's Horizon 2020 research and innovation programme (grant agreement 682754 to E.L.).

Declaration of interests. The authors report no conflict of interest.

Data availability statement. The data that support the findings of this study are openly available upon request to C. Kamal.

Author ORCIDs.
Catherine Kamal https://orcid.org/0000-0003-2813-0619;
Eric Lauga https://orcid.org/0000-0002-8916-2545.

References

Arrigo, K.R., Robinson, D.H., Worthen, D.L., Dunbar, R.B., DiTullio, G.R., VanWoert, M. & Lizotte, M.P. 1999 Phytoplankton community structure and the drawdown of nutrients and CO_2 in the Southern Ocean. *Science* **283**, 365–367.

Batchelor, G.K. 1970 Slender-body theory for particles of arbitrary cross-section in Stokes flow. *J. Fluid Mech.* **44**, 419–440.

Brennen, C. & Winet, H. 1977 Fluid mechanics of propulsion by cilia and flagella. *Annu. Rev. Fluid Mech.* **9**, 339–398.

Burgers, J.M. 1938 On the motion of small particles of elongated form suspended in a viscous liquid. *Kon. Ned. Akad. Wet. Verhand.(Eerste Sectie)* **16**, 113–184.

Coppola, S. & Kantsler, V. 2021 Green algae scatter off sharp viscosity gradients. *Sci. Rep.* **11**, 1–7.

Cox, R.G. 1970 The motion of long slender bodies in a viscous fluid. Part 1. General theory. *J. Fluid Mech.* **44**, 791–810.

Cox, R.G. 1971 The motion of long slender bodies in a viscous fluid. Part 2. Shear flow. *J. Fluid Mech.* **45**, 625–657.

Dandekar, R. & Ardekani, A.M. 2020 Swimming sheet in a viscosity-stratified fluid. *J. Fluid Mech.* **895**, R2.

Daniels, M.J., Longland, J.M. & Gilbart, J. 1980 Aspects of motility and chemotaxis in spiroplasmas. *Microbiology* **118**, 429–436.

Datt, C. & Elfring, G.J. 2019 Active particles in viscosity gradients. *Phys. Rev. Lett.* **123**, 158006.

Du Roure, O., Lindner, A., Nazockdast, E.N. & Shelley, M.J. 2019 Dynamics of flexible fibers in viscous flows and fluids. *Annu. Rev. Fluid Mech.* **51**, 539–572.

Eastham, P.S. & Shoele, K. 2020 Axisymmetric squirmers in Stokes fluid with nonuniform viscosity. *Phys. Rev. Fluids* **5**, 063102.

Greenberg, E.P. & Canale-Parola, E. 1977 Motility of flagellated bacteria in viscous environments. *J. Bacteriol.* **132**, 356–358.

Guadayol, Ò., Mendonca, T., Segura-Noguera, M., Wright, A.J., Tassieri, M. & Humphries, S. 2021 Microrheology reveals microscale viscosity gradients in planktonic systems. *Proc. Natl Acad. Sci. USA* **118** (1), e2011389118.

Guyon, E., Hulin, J.-P., Petit, L. & Mitescu, C.D. 2015 *Physical Hydrodynamics*. Oxford University Press.

Han, K., Shields IV, C.W. & Velev, O.D. 2018 Engineering of self-propelling microbots and microdevices powered by magnetic and electric fields. *Adv. Funct. Mater.* **28**, 1705953.

Kim, S. & Karrila, S.J. 2013 *Microhydrodynamics: Principles and Selected Applications*. Courier Corporation.

Koens, L. & Lauga, E. 2017 Analytical solutions to slender-ribbon theory. *Phys. Rev. Fluids* **2**, 084101.

Lauga, E. 2020 *The Fluid Dynamics of Cell Motility*. Cambridge University Press.

Laumann, M. & Zimmermann, W. 2019 Focusing and splitting streams of soft particles in microflows via viscosity gradients. *Euro. Phys. J.* E **42**, 1–11.

Li, G., Lauga, E. & Ardekani, A.M. 2021 Microswimming in viscoelastic fluids. *J. Non-Newtonian Fluid Mech.* **297**, 104655.

Liebchen, B., Monderkamp, P., Ten Hagen, B. & Löwen, H. 2018 Viscotaxis: microswimmer navigation in viscosity gradients. *Phys. Rev. Lett.* **120**, 208002.

López, C.E., Gonzalez-Gutierrez, J., Solorio-Ordaz, F., Lauga, E. & Zenit, R. 2021 Dynamics of a helical swimmer crossing viscosity gradients. *Phys. Rev. Fluids* **6**, 083102.

Mirbagheri, S.A. & Fu, H.C. 2016 *Helicobacter pylori* couples motility and diffusion to actively create a heterogeneous complex medium in gastric mucus. *Phys. Rev. Lett.* **116**, 198101.

Ottemann, K.M. & Lowenthal, A.C. 2002 *Helicobacter pylori* uses motility for initial colonization and to attain robust infection. *Infect. Immun.* **70**, 1984–1990.

Petrino, M.G. & Doetsch, R.N. 1978 'Viscotaxis', a new behavioural response of *Leptospira interrogans* (*biflexa*) strain B16. *Microbiology* **109**, 113–117.

Shaik, V.A. & Elfring, G.J. 2021 Hydrodynamics of active particles in viscosity gradients. *Phys. Rev. Fluids* **6**, 103103.

Stehnach, M.R., Waisbord, N., Walkama, D.M. & Guasto, J.S. 2021 Viscophobic turning dictates microalgae transport in viscosity gradients. *Nat. Phys.* **17**, 926–930.

Swidsinski, A., Sydora, B.C., Doerffel, Y., Loening-Baucke, V., Vaneechoutte, M., Lupicki, M., Scholze, J., Lochs, H. & Dieleman, L.A. 2007 Viscosity gradient within the mucus layer determines the mucosal barrier function and the spatial organization of the intestinal microbiota. *Inflamm. Bowel Dis.* **13**, 963–970.

TAKABE, K., TAHARA, H., ISLAM, M.S., AFFROZE, S., KUDO, S. & NAKAMURA, S. 2017 Viscosity-dependent variations in the cell shape and swimming manner of *Leptospira*. *Microbiology* **163**, 153–160.

TAYLOR, G.I. 1967 Film notes for low-Reynolds-number flows. *Rep*. 21617. National Committee for Fluid Mechanics Films.

TILLETT, J.P.K. 1970 Axial and transverse Stokes flow past slender axisymmetric bodies. *J. Fluid Mech.* **44**, 401–417.

TUCK, E.O. 1964 Some methods for flows past blunt slender bodies. *J. Fluid Mech.* **18**, 619–635.

WHEELER, K.M., CÁRCAMO-OYARCE, G., TURNER, B.S., DELLOS-NOLAN, S., CO, J.Y., LEHOUX, S., CUMMINGS, R.D., WOZNIAK, D.J. & RIBBECK, K. 2019 Mucin glycans attenuate the virulence of *Pseudomonas aeruginosa* in infection. *Nat. Microbiol.* **4**, 2146–2154.